Role of Entry Barriers in the Foam Destruction by Oil Drops

Asen Hadjiiski, Nikolai D. Denkov, Slavka Tcholakova, Ivan B. Ivanov*

Laboratory of Chemical Physics Engineering

(Formerly Laboratory of Thermodynamics and Physico-chemical Hydrodynamics)

Faculty of Chemistry, Sofia University

1 James Bourchier Ave., 1164 Sofia, BULGARIA

***Correspondence to:**

Professor Ivan B. Ivanov

Laboratory of Chemical Physics Engineering

Faculty of Chemistry, Sofia University

1 James Bourchier Ave.

1164 Sofia, BULGARIA

Phone: (+359) 2-962 5310

Fax: (+359) 2-962 5643

E-mail: II@LTPH.BOL.BG

Abstract

Different oils (mainly hydrocarbons or silicone oils) and their mixtures with hydrophobic solid particles are widely used for destruction of undesirable foam. For a long time, the entry, E, spreading, S, and bridging, B, coefficients (which can be calculated from the interfacial tensions oil-water, oil-air and water-air) were used to evaluate the activity of such oil-based antifoams (AF). However, recent studies showed that there is no correlation between the magnitudes of E, S, B and the antifoam activity - the only requirement for having an active AF, in this aspect, is to have positive E and B. Instead, it was shown that the so called "entry barrier", which characterizes the facility of entry of pre-emulsified oil drops on the solution surface, is of crucial importance - an easy entry (low entry barrier) corresponds to active AF and vice versa. We developed recently a new method, the Film Trapping Technique (FTT), which allows one for first time to measure directly the critical capillary pressure, P_C^{CR}, which induces the entry of micrometer sized oil drops, identical to those in real AFs. This article describes the main results, obtained so far by the FTT with various systems. The results evidence that P_C^{CR} can be used as a relevant quantitative characteristic of the entry barrier. The value of P_C^{CR} determines the boundary between two rather different classes of AF: fast antifoams (defoaming time < 5 s, P_C^{CR} < 20 Pa) and slow antifoams (defoaming time > 5 min, P_C^{CR} > 20 Pa). These two classes differ in the mechanism, by which they destroy foam - the fast AF destroys the foam films in the first several seconds after their formation, whereas the drops of the slow AF destroy the foam only after being compressed by the walls of the shrinking Gibbs-Plateau borders, at a much later stage of foam evolution. Furthermore, a linear relationship between the value of P_C^{CR} and the final height of the foam is established and explained theoretically for the slow AFs. The effects of several factors (type of oil, size of the oil drops, surfactant concentration, presence of a spread oil layer over the solution surface) on the entry barrier are studied. It is shown for one specific system that the presence of a pre-spread oil layer on the solution surface affects strongly the entry barrier - the latter is reduced by the spread layer for decane and dodecane, whereas the effect is the opposite for hexadecane (fivefold increase). The calculations show that there is a big difference between the numerical values of the critical *capillary* pressure, P_C^{CR}, and the critical *disjoining* pressure, Π_{AS}^{CR}, for micrometer sized oil drops - therefore, one should analyze separately the relation between these two quantities and the antifoam activity. In conclusion, the FTT has provided a valuable new information about the role of entry barrier in the activity of oil-based antifoams.

I. Introduction.

Oily additives are used in various technologies (e.g., paper and pulp production, ore flotation, fermentation) and commercial products (detergents, paints, some pharmaceuticals) to avoid the formation of an excessive foam, which would impede the technological process or the product application [1-3]. In other cases (oil recovery and refinement, shampoos, emulsions for metal processing machines) oil drops are present, without being specially introduced for foam control, and can also affect the foamability of the solutions. Small fractions of hydrophobic solid particles of micrometer size, such as hydrophobized silica or alumina, plastic grains, or stearates of multivalent cations, are often pre-mixed with the oil, because the obtained solid-oil "compounds" exhibit much stronger foam destruction effect than the individual components taken separately [4-8]. Such oily additives are termed "antifoams" in the literature and can be based on hydrocarbons, polydimethylsiloxanes (PDMS, silicone oil) or their derivatives [1, 4].

The mechanisms by which oil drops destroy foams are still a matter of discussion in the literature [2-15]. Two of the possible mechanisms (called "bridging-stretching" and "bridging-dewetting") are illustrated in Figure 1. Observations by optical microscope and high-speed video camera showed that the bridging-stretching mechanism is operative when compounds of silicone oil and silica are applied to some surfactant solutions [11]. Several of the mechanisms, proposed in the literature, relate the antifoam activity of the oil to its spreading behavior (see the respective discussion in Refs. 4, 5 and the literature cited therein). The so called entry, E, spreading, S, and bridging, B, coefficients (which can be calculated from the interfacial tensions air-water, air-oil, and oil-water) have been often invoked to characterize the oils with respect to their antifoam properties. However, several recent studies [4, 9, 13-17] demonstrated that there is no direct relation between the values of these coefficients and the antifoam activity of the oils. Instead, a correlation between the antifoam activity and the so called "entry barrier", which characterizes the facility of oil drop entry on the surface of the surfactant solution (see below for quantitative definitions), has been established. The primary reason for this correlation is that whatever the mechanism of foam destruction by emulsified oil might be, it must include the stage of formation and rupture of asymmetric oil-water-air films (see Figure 1). As noticed long ago by Kruglyakov [18] and Kulkarni et al. [19], these asymmetric films can be stabilized by various surface forces (electrostatic, van der Waals, etc.), which hinder or suppress the drop entry and thus impede the antifoam action of the oil. Later on, Wasan and coworkers [3, 10] studied the importance of the oscillatory structural forces for the stability of the asymmetric films formed from surfactant solutions with concentration well above their critical micelle concentration (CMC). Furthermore, they showed that the introduction of oil into the foaming solution might lead to a more stable foam due to decelerated water drainage, as a result of the Plateau border obstruction by the oil drops, if the asymmetric film is very stable [20].

Several different characteristics have been suggested in the literature to quantify the entry barriers for oil drops. Lobo and Wasan [10] suggested to use the energy of interaction per unit area in the asymmetric oil-water-air film, f, as a criterion of its stability:

$$f(h_E) = -\int_{h\to\infty}^{h_E} \Pi_{AS}\, dh \qquad (1)$$

where $\Pi_{AS}(h)$ is the disjoining pressure, while h_E is the equilibrium thickness of the asymmetric film at a certain capillary pressure. Bergeron et al. [9] suggested the so-called generalized entry

coefficient

$$E_g(h_E) = -\int_0^{\Pi_{AS}(h_E)} h \, d\Pi_{AS} \tag{2}$$

where the lower limit of the integral corresponds to $\Pi_{AS}(h \to \infty) = 0$. As seen from their definitions, eqs 1 and 2, f and E_g are closely interrelated

$$E_g(h_E) + f(h_E) = -h_E \, \Pi_{AS}(h_E) \tag{3}$$

The determination of the values of f and E_g, and their comparison with the antifoam efficiency of different oils is a difficult task, because one needs to know the dependence of the disjoining pressure, Π_{AS}, on the thickness of the asymmetric film for the entire range - h varying from infinity to h_E. The most thorough analysis of this type was carried out by Bergeron et al. [9] who measured the disjoining pressure isotherms of planar foam (air-water-air) and asymmetric (oil-water-air) films by the "porous plate method" [21] and determined E_g for two surfactant-oil couples. Although a qualitative agreement between the values of E_g and the foam stability was established, a rigorous quantitative comparison for all systems was impossible, because one cannot measure the attractive regions of the isotherms $\Pi_{AS}(h)$ by the porous plate method.

One important result of that study [9] was that the authors convincingly proved that the destabilizing effect of oil is related to much lower stability of the asymmetric films as compared to the stability of the foam films. Furthermore, a good correlation was found between the stability of foams, which were formed in porous media in the presence of oil (thus resembling the foams in oil reservoirs) and the critical capillary pressure leading to rupture of the asymmetric films, as measured by the porous plate method. Indeed, the critical capillary pressure seems to be the most adequate measure of the film stability in such systems, because the capillary pressure is the actual external variable that compresses the film surfaces toward each other, against the repulsive surface forces (disjoining pressure) stabilizing the film. It is worth noting that the quoted authors [9] studied *planar* films, where the imposed capillary pressure in equilibrium is exactly equal to the stabilizing disjoining pressure - that is, the concept of the critical *capillary pressure*, P_C^{CR}, is equivalent to the concept of the critical *disjoining pressure*, Π_{AS}^{CR}, in their studies. As explained below, the asymmetric films formed in typical antifoam systems are strongly curved and there is a big difference between the values of P_C^{CR} and Π_{AS}^{CR}.

Recently, another experimental tool became available for quantifying the entry barriers of oil drops. Hadjiiski et al. [17, 22-25] developed a new method, the Film Trapping Technique (FTT), which consists in trapping oil drops in a wetting film, formed from surfactant solution on a solid substrate, and a subsequent measurement of the critical capillary pressure that leads to drop entry on the fluid surface of the wetting film (see below for details). The FTT has several advantages as compared to the porous plate method: First, experiments with real antifoam drops of micrometer size can be carried out, giving a quantitative measure of the entry barrier that can be used to explain the antifoam activity [13-17]. Second, the FTT allows an independent variation of the radius of the asymmetric oil-water-air film and of the applied capillary pressure, i.e. the dependence of P_C^{CR} and Π_{AS}^{CR} on the size of the asymmetric film can be investigated. Third, the method can be applied to different types of film (asymmetric oil-water-air, emulsion and foam films), so that a comparison of their stability for a given surfactant-oil system is possible. Last but not least, the FTT requires a relatively simple and cheap equipment, and after

accumulating some experience one can rapidly obtain a large set of data. These features make the method an interesting complement and/or alternative to the other methods for studying liquid films.

In this article we present a brief overview of the results obtained so far by the FTT with various oils and surfactants in relation to antifoaming. As shown below, the critical capillary pressure, determined in the FTT experiments, has a close relation to the actual process of foam destruction by oil drops. Several conclusions about the mechanism of antifoaming and the antifoam activity of the oils, have been drawn and presented in quantitative terms by using the concept of the critical capillary pressure, P_C^{CR}, and the FTT results.

II. Experimental details.

A. Materials. Sodium dioctylsulfosuccinate, AOT (Sigma Chemical Co., St. Louis, MO, USA); octylphenol decaethylene glycol ether, Triton X-100 (Merck KGaA, Darmstadt, Germany); alkyl-$C_{12/14}$ (glucopiranoside)$_{1.2}$, APG (Henkel KGaA, Germany); sodium dodecyl polyoxyethylene sulfate, SDP3S (Kao Co., Tokyo, Japan); sodium dodecyl benzene sulfonate, SDDBS (Aldrich, Steinheim, Germany); and sodium dodecyl sulfate, SDS (Sigma) are used as surfactants. In two series of experiments lauryl amide propyl betaine, Betaine (Kao) and n-dodecanol, n-C_{12}OH (Sigma), are added to SDP3S and SDS solutions, respectively, as foam boosters. The compositions of the studied surfactant solutions are summarized in Table 1.

The following oils are studied: n-octane, n-C_8; n-decane, n-C_{10}; n-dodecane, n-C_{12}; n-hexadecane, n-C_{16}; n-dodecanol, n-C_{12}OH (all products of Sigma); and two silicone oils (poly-dimethylsiloxane, PDMS) of different dynamic viscosity: 5 mPa.s and 1000 mPa.s.

A mixed, solid-oil compound is also used as an antifoam, which consists of 4.2 wt % hydrophobized silica particles dispersed in PDMS of viscosity 1000 mPa.s. The oil concentration in the working solutions is 0.1 wt % for pure oils and 0.01 wt % for mixed solid-oil compounds.

Hexadecane is refined by passing it through a glass column filled with chromatographic adsorbent (Florisil). The other chemicals are used as received. The solutions are prepared with deionized water from Milli-Q Organex system (Millipore).

B. Methods and procedures.

1. Foam formation and foam stability evaluation.

Since the solid-oil compounds destroy the entire foam column within several seconds, while the pure oils are much slower (minutes and dozens of minutes), different tests are used to produce foams and to compare their stability in the presence of various antifoams.

a. Ross-Miles test. This test is appropriate for studying the antifoam action of pure oils [13, 14]. Briefly, 0.3 mL of oil is introduced into 300 mL of the surfactant solution. The oil is emulsified in the solution by intensive stirring for 20 min on a magnetic stirrer. The obtained emulsion is additionally homogenized by several hand-shakes before placing it into the glass cylinder of the Ross-Miles test. The cylinder has a working volume of 1 dm^3 and diameter of 37 mm. The solution is circulated (pumped) for 20 seconds at a debit of 125 cm^3/s through an orifice (7 mm in diameter), which is placed at 23 cm above the level of the liquid. The volume of the initially formed foam and the evolution of the foam volume with time is monitored for a period of 15 min (100 min in some of the experiments) after ceasing the liquid circulation. The accuracy in the foam volume determination is ± 2 mL (determined mainly by the irregular upper

boundary of the foam), whereas the reproducibility is typically ± 5 mL.

b. Automated Shake Test (AST). This test is appropriate for evaluating the antifoam activity of solid-oil compounds [6, 11, 15]. The tests are performed on an automatic shake-machine Agitest (Bioblock). 100 mL of the foaming solution is placed in a standard 250 mL glass bottle, and 0.01 mL of the compound is introduced into this sample. The bottle is then mechanically agitated by the machine, at a frequency of 360 min^{-1} and an amplitude of 2 cm. After 10 s of agitation, the shaking is ceased and the time for complete foam destruction (defoaming time) is monitored for a period, which does not exceed 60 s. A micropipette Nichiryo M800 (Nichiryo Co., Tokyo, Japan), which is specially designed to supply small volumes of viscous substances, is used to load the compound.

2. Methods for studying foam films.

Several complementary methods are used to observe the process of foam film thinning and destruction in the presence of antifoam globules.

a. Capillary cell. Single, millimeter-sized foam film is formed by the method of Scheludko and Exerova [26, 27]. A drop of surfactant solution (sometimes containing dispersed antifoam drops) is placed in a short capillary tube with an internal diameter of 2.5 mm. The drop acquires a biconcave shape with the thinnest region being in the center of the capillary. The foam film is formed by sucking out liquid from the drop through a side orifice, drilled in the capillary wall. This film is observed in reflected monochromatic light by a microscope (Zeiss Axioplan, Germany; objectives Plan-Neofluar, 10×/0.30; LD Epiplan, 20×/0.40). The image is recorded by a CCD camera (Panasonic WV-CD20, 25 fps). The interference of the light, reflected from the upper and lower surfaces of the foam film, leads to the appearance of dark and bright interference fringes, each of them corresponding to a given film thickness. The difference, Δh, in the film thickness between two neighboring dark (or two neighboring bright) fringes is equal to

$$\Delta h = \lambda / 2n \approx 203 \text{ nm} \tag{4}$$

where $\lambda \approx 540$ nm is the wavelength of the illuminating light, and $n = 1.33$ is the refractive index of the surfactant solution.

A major advantage of the capillary cell is that experiments can be performed with surfactant solutions containing micrometer sized oil globules or lenses, just as in the case for practical antifoams [11, 28]. Thus, the films in the capillary cell closely mimic the behavior of relatively small films (of diameter around 1 mm) in real foams.

b. Dippenaar cell [29]. We use this technique to observe the evolution of the oil bridge, which forms when an oil drop comes in a direct contact with the two surfaces of a foam lamella [11]. Similarly to the experiments in the capillary cell, the foam lamella is formed between two concave menisci in a short capillary tube (4 mm internal diameter). The lamella thickness is controlled by sucking liquid through a side orifice. The placement of an antifoam drop (≈ 2 μL in volume) on the upper meniscus leads to the formation of an oil lens, floating on the solution surface. When the bottom of this lens touches the lower air-water meniscus, an oil bridge can be formed. The shape of the oil bridge is monitored in transmitted white light. The main advantage of the Dippenaar cell is the possibility for direct optical observation of the bridge shape.

3. Film Trapping Technique (FTT).

a. Experimental setup and basic principles of operation. The critical capillary pressure leading to entry of the oil drops is measured by the FTT [25], see Figure 2. A vertical glass capillary, of radius 4 mm, is positioned at a small distance above the flat bottom of a glass

vessel. The lower end of the capillary is immersed in the working surfactant solution, which contains dispersed antifoam globules. The capillary is connected to a pressure control system, which allows one to vary and to measure the difference, ΔP_A, between the air pressure in the capillary, P_A, and the ambient atmospheric pressure, P_A^0. The data acquisition equipment includes a pressure transducer (Omega Engineering, Inc., Stamford, U.S.A.) and a digital multimeter Metex M-4660A (Metex Instruments) connected to a computer (PC).

When P_A increases, the air-water meniscus in the capillary is pushed against the glass substrate and a wetting film is formed, which traps some of the antifoam globules (Figure 2B). These drops remain sandwiched between the air-water meniscus and the glass substrate. The setup allows one to measure the capillary pressure of the air-water meniscus around the trapped drops, which can be expressed by the following relationship

$$P_C = \Delta P_A - \rho_W g Z \,, \tag{5}$$

where the second term on the right-hand side of the equation accounts for the hydrostatic pressure at the bottom of the vessel. The depth of the liquid, Z, is measured by a micrometer translator having an accuracy of ±5 μm, which corresponds to precision of ± 0.05 Pa in the determination of the hydrostatic pressure. A Carl Zeiss Jena inverted microscope, equipped with objective LD Epiplan, 20×/0.40, digital CCD camera (Kappa CF 8/1 DX) connected to a PC and VCR (Panasonic NV-HD 680), is used for these observations.

The experiments show that the trapped antifoam globules enter (pierce) the surface of the wetting film at a given, critical capillary pressure, P_C^{CR}. The moment of drop entry, which is accompanied with a significant local change in the shape of the air-water interface, is clearly seen in both reflected and transmitted light. Therefore, the equipment allows one to measure P_C^{CR} as a function of the solution composition and drop radius. As mentioned above, for brevity we refer to P_C^{CR} as to *the barrier to drop entry*. Larger P_C^{CR} corresponds to higher barriers (more difficult drop entry) and vice versa.

b. FTT - gentle. The experimental setup described above allows one to measure the entry barriers higher than ca. 20 Pa. This limit is determined by the capillary pressure of the meniscus formed in the capillary before trapping the drops. Since the surfactant solution wets the inner surface of the capillary, a spherical meniscus is formed of capillary pressure $P_C \approx 2\sigma_{AW}/R_{CAP} \sim$ 15 Pa ($\sigma_{AW} \approx 30$ mN/m is the surface tension of the solution and $R_{CAP} \approx 4$ mm is the capillary radius). However, the entry barriers are sometimes lower and another modification of the method, called "gentle FTT", has been developed [25] for such cases, Figure 2C.

The main idea of the gentle FTT is to create an almost flat air-water interface in the capillary before trapping the drops, so that P_C in the beginning of the experiment is virtually zero. For this purpose, a sapphire disc of special design is attached to the lower end of the capillary. The disc has an opening with a wedge-like shape (Figure 2C), which ensures a stable attachment of the air-water interface to the sapphire upper edge. Additionally, a substrate with a small stub, cut out onto a glass plate, is used in these experiments. The plate is placed on the vessel's bottom, so that the stub is projected upward into the opening of the sapphire. One can move precisely the capillary in the *x-y-z* directions and to juxtapose the flat fluid interface with the glass stub. Thus one can achieve trapping of drops by a flat interface, followed by a gentle increase of P_C until P_C^{CR} is reached.

c. Drop entry measurements in the absence of a spread oil layer. The working surfactant solutions, containing oil-based antifoams, usually have a spread layer of oil on their surface, as a

result of the coalescence of antfioam globules with this surface [11]. Some of the experiments are aimed to reveal what is the effect of this pre-spread oil layer on the height of the entry barrier. For this purpose comparative experiments, in the presence and in the absence of spread oil, are performed with solutions of the anionic surfactant SDDBS and several oils.

For oils that are not very much soluble in the surfactant solution, like dodecane and hexadecane, a clean surface (free of spread oil) is created by pouring the studied emulsions into the experimental vessel for FTT experiments by the "two-tips procedure", TTP [11]. The latter consists in a gentle injection of the solution, containing emulsified oil drops, through a narrow orifice (syringe needle or pipette tip) into the working vessel - in this way the oil layer, spread on the surface of the "mother" emulsion, is retained and a clean solution surface is created for the FTT experiment. It takes some time, which depends very much on the used oil and surfactant, before a new portion of spread oil appears due to coalescence of oil drops with the solution surface or to molecular transfer of oil [11,17]. Independent surface tension measurements reveal that for dodecane and hexadecane the value of σ_{AW} of the emulsions poured by the TTP is virtually the same as that of the pure SDDBS solution (without oil) and decreases very slowly with time - by less than 0.5 mN/m for a period of 1 h, which is about the time-span of the typical FTT experiment. In these FTT tests, the number of the drop entry events observed in a single experiment is restricted to 6, to avoid the accumulation of detectable layer of spread oil from the entering drops.

For oils that are soluble in water and/or solubilized in the surfactant micelles (such as octane, dodecanol), it is impossible to create a solution surface free of spread oil for a period of time, long enough to accomplish the FTT experiments. In these systems, the entry barrier is measured only in the presence of spread oil.

All experiments are carried out at the ambient room temperature ($T = 25 \pm 2$ °C). The experiments with dodecanol are performed at temperature above its melting point (m.p. = 24 °C). The water evaporation inside the capillary is avoided by saturating the atmosphere above the wetting film with aqueous vapors.

4. Surface tension measurements. The surface tension of the surfactant solutions is measured by the Wilhelmy plate method, whereas the surface tension of the oils is measured by Du Nouy ring technique on Krüss K10T digital tensiometer. The interfacial tension of the oil-solution interfaces is measured by the pendant drop method.

III. Experimental Results and Discussion.

A. Relation between the Drop Entry Barrier and the Antifoam Activity.

1. Drop Entry Barrier and Foam Lifetime - Fast and Slow Antifoams. A careful look on the results published in the literature [1-8, 30] and our own foam tests (refs 11, 13-16 and some new results presented below), demonstrate a segregation of the antifoam systems into two distinct groups, depending on the time-scale of foam destruction. Some of the antifoams (usually these are mixed solid-oil compounds) are very active and destroy the entire foam column for less than 10 s [3, 6, 11, 15]. On the other hand, oils deprived of solid particles typically require much longer time (at least several minutes) to destroy a significant fraction of the foam [8, 13-16, 20]. For example, 0.01 wt % of silica-PDMS compound destroys completely the foams stabilized by AOT (10 mM) or Triton X-100 (1 mM) for 2-3 seconds in the Automatic Shake Test, while the same silicone oil, when deprived of silica, has a very slow action and several minutes elapse

between the foam generation and the beginning of the foam destruction process. Moreover, if pure oil is used, the foam destruction is incomplete and a long standing residual foam often remains stable for hours. To distinguish these two types of antifoam, we call them "fast" and "slow", respectively [15].

To clarify the actual reason for the different activity of the fast and slow antifoams, we performed a large set of experiments aimed to reveal the relation between the entry barrier and the characteristic defoaming time. As an illustration of the obtained results, let us discuss first the FTT experiments with 10 mM AOT solutions. Two antifoam systems are compared: (i) pure silicone oil of viscosity 1000 mPa.s, and (ii) compound comprising the same oil and hydrophobic silica particles. The gentle-FTT setup is used for these measurements, because some of the entry barriers are rather low.

The results for the critical capillary pressure, P_C^{CR}, as a function of the equatorial radius of the antifoam drops, R_E, are shown in Figure 3. The triangles present the results for P_C^{CR} measured with compound globules, whereas the empty circles show data for pure oil drops. The two horizontal lines represent the respective averaged values for a given antifoam. As seen from the figure, the magnitude of the entry barrier does not depend significantly on the drop size in the studied range (typical for real antifoams). On the other side, the mean entry barrier for pure oil is about 20 Pa, whereas it is much lower for the mixed solid-oil antifoam, about 1 Pa. Therefore, the introduction of hydrophobic silica into the oil leads to a significant decrease of the entry barrier, by a factor of 20. As mentioned above, this reduction is accompanied by a very strong acceleration of the foam destruction process. These results reinforce the hypothesis of Garrett [4], supported already by the experiments of Bergeron et al. [6], Koczo et al. [7], and Aveyard and Clint [8], that the main role of the solid particles in mixed solid-oil antifoams is to reduce the entry barrier of the antifoam globules.

Further, we performed similar experiments with a variety of different systems - oils, compounds, and surfactant solutions. The results are summarized in Figure 4, which shows the relationship between the foam lifetime and the entry barrier. Each experimental point corresponds to a different surfactant-antifoam couple (see the figure caption for specification of the studied systems). One sees that the experimental data fall into two distinct regions: (1) Systems where the foam is destroyed for less than 5 s (fast antifoams). For all of these systems the entry barrier is below 15 Pa; (2) Systems where the defoaming time is longer than 8 min (slow antifoams), for which the entry barrier is above 20 Pa. One can conclude that there is a well-defined threshold value of the entry barrier, somewhere between 15 and 20 Pa, which separates the region of the fast antifoams from the region of the slow ones. Therefore, the magnitude of the entry barrier, P_C^{CR}, is of crucial importance for the time scale of foam destruction by a given antifoam.

As shown below, the threshold value of P_C^{CR} is related to a transition from one mechanism of foam destruction (rapid rupture of the foam films) to another, much slower mechanism, which includes a compression of the antifoam globules in the Gibbs-Plateau borders of the foam.

2. Observations of single foam films - position of drop entry. One important question for any mechanism of foam destruction by oils is which structural element of the foam (foam film or Gibbs-Plateau border) is actually destroyed by the antifoam globules. Most of the mechanisms, discussed in the literature [2, 4, 6, 11, 12, 18], imply that the *foam films* are ruptured by the antifoams, because these films rapidly thin down to thickness comparable to the globule diameter (on the order of a micrometer). On the other side, Koczo et al. [7] suggested that the antifoam globules may first escape from the foam films into the neighboring *Gibbs-Plateau*

borders (GPBs) and get trapped there. According to these authors, the antifoam globules are compressed by the walls of the narrowing GPBs, where eventually the drop entry occurs and the foam is destroyed. Our experiments have shown that both scenarios can be realized depending on the particular system [11, 13, 14]. However, the actual reason for the different location of the antifoam action has not been clarified so far. Therefore, we performed systematic experiments for investigation of the relationship between the entry barrier and the structural element (foam film or GPB), where the globule entry occurs.

The capillary cell provides the possibility for a direct check whether the antifoam ruptures the foam films [11, 13]. We observed the process of thinning (and sometimes rupture) of foam films of diameter 0.7 ± 0.1 mm, in the presence of dispersed globules of fast or slow antifoams. We describe below, as an example, the foam films formed from 10 mM AOT and 0.1 M SDP3S solutions - the results for the other studied systems of low molecular surfactants are very similar.

a. Films without antifoam globules. Let us first describe briefly the main stages of foam film thinning in the absence of antifoam. Immediately after its formation, the foam film has a non-uniform thickness with a lens-shaped thicker region (called "dimple") in its central part - see Figure 5. The thickness in the dimple center is typically 3 to 4 μm, while the thickness is about 1 μm in the film periphery. The dimple is hydrodynamically unstable and the liquid captured in it spontaneously leaves the film (by an asymmetric outflow) within a few seconds. Afterwards, the film surfaces become approximately plane-parallel with several channels (dynamic regions of thickness 200-500 nm larger than the main planar portions of the film) spanning across the film area. The film gradually thins down to 100 nm for less than a minute, and the channels almost disappear. Further, several consecutive stepwise transitions in the film thickness are observed, which occur through formation and expansion of thinner spots. Such a multi-step film thinning is called "stratification" in the literature and is due to the oscillatory structural forces created by the surfactant micelles [31-36]. About 2-3 min after its formation, the foam film reaches its final thickness (10-20 nm, which corresponds to a common black film) and remains stable for many hours in the absence of antifoam.

The stages of foam film thinning described above are typical for the aqueous solutions of most low molecular surfactants, and the time-scale of the process is approximately the same - the film thickness becomes on the order of 1 μm for several seconds, about 1 min is needed for thinning of the film down to about 100 nm, and 2 to 4 min - until the final equilibrium film thickness is established. The main difference between the various systems is in the number of the step-wise transitions, which strongly depends on the surfactant concentration. Close to the critical micelle concentration (CMC), when the volume fraction of the micelles is low, there is either only one transition from a common black film to a very thin Newton black film, or there are no transitions at all, because the equilibrium film thickness corresponds to a common black film, stabilized by electrostatic or steric forces. However, when the surfactant concentration is well above the CMC, up to 5-7 transitions are observed due to the multiple barriers in the disjoining pressure curve $\Pi(h)$, which are caused by the oscillatory structure forces [34-36].

b. Films containing drops of pure silicone oil. The films formed in the capillary cell from solutions containing drops of pure silicone oil are rather stable, similarly to the films formed in the absence of antifoam. The film-thinning behavior is slightly affected by the presence of the oil drops, and the same stages are observed in approximately the same time scale. Microscopically one can see that several oil drops are usually captured in the dimple, immediately after film formation. Most of these drops leave the foam film together with the dimple. The drops, which remain in the foam film after dimple expulsion, move from the planar film areas toward the

channels (where the film thickness is larger) and then leave the film, following the drainage of liquid through the channels. At a film thickness of around 100 nm and below, no oil drops remain in the film because the latter is thinner than the diameter of the smallest drops. Therefore, the foam film is deprived of oil drops during the later stages of its thinning, because the drops are expelled into the thicker meniscus region, which surrounds the film - Figure 6.

The fact that the real foams containing oil drops are unstable (though at least several minutes are needed before the foam destruction starts), while the foam films in the capillary cell remain stable for much longer time, indicates that the mechanism of foam destruction by oil drops does not occur through rupture of the foam films. Another mechanism, which is in agreement with the available results for these systems is discussed in sections III.A.4 and III.A.5.

c. Films containing mixed solid-oil antifoam globules. The stages and the time scale of film thinning are almost the same, as in the experiments described above, with one important exception - in most cases the antifoam globules induce a rupture of the foam film in the early stages of its thinning (1 to 10 s) at a relatively large thickness (≈ 1 μm). One important feature of the observed process is the formation of a characteristic interference pattern, clearly seen with a high-speed video camera [11], just before the film rupture. This interference pattern, called by us "fish-eye", because of its appearance, corresponds to a local reduction of the film thickness by 100 to 300 nm - see Figure 7. This reduction of the local film thickness is due to the formation of an oil bridge between the two foam film surfaces - see Figure 8 and section III.A.3 below. The film region, perturbed by the oil bridge, is relatively small (10-50 μm in diameter) and the rest of the foam film thins without being notably affected by the bridge [11, 12]. Typically, the foam film ruptures soon (from several milliseconds up to several seconds) after the formation of the first fish-eye. In most of the cases, one can specify exactly which antifoam globule became a bridge.

The process of hole formation and expansion inside the foam films was directly observed with larger vertical foam films (2×3 cm^2) by using a high-speed video camera [11]. 10 mM AOT solutions and silica-PDMS compound were used in these experiments. The results unambiguously demonstrated that the fast antifoams rupture the foam films (not the GPBs). Most of these large films ruptured almost immediately (within 0.5 s) after their formation at a thickness of several micrometers.

3. Foam destruction by fast antifoams - bridging-stretching mechanism of foam film rupture. The fact that the foam films are destroyed almost immediately after the formation of an oil bridge, shows that these bridges are unstable. The microscopic observations [11] and the theoretical analysis [12] showed that once formed, the oil bridge stretches with time due to uncompensated capillary pressures at the oil-water and oil-air interfaces, and eventually ruptures, leading in this way to a destruction of the entire foam film. This mechanism of foam film rupture, called "bridging-stretching" [11, 12], is illustrated in Figure 8 by schematic drawing and by photographs taken in the Dippenaar cell with 10 mM AOT solutions and silica-PDMS compound. As seen from the figure, the oil bridge acquires a shape with concave oil-water interfaces and the thinnest region is in the bridge center. By changing the amount of the surfactant solution in the Dippenaar cell, we are able to stretch the bridge in radial direction, which eventually causes its rupture and destruction of the entire foam film. The conditions for stability of oil bridges, along with the details of the bridging-stretching mechanism are discussed in Ref. [12].

The bridging-stretching process is an alternative to another possible scenario for foam film destruction [3-8], which implies that the antifoam globules are dewetted by the surfactant solution ("bridging-dewetting" mechanism, Figure 1). One cannot exclude the possibility that in

other systems the antifoam globules destroy the foam films by the bridging-dewetting mechanism.

4. Foam destruction by slow antifoams (Figure 9). As explained above, the globules of the slow antifoams escape from the foam films and accumulate in the GPBs, as suggested by Koczo et al. [7]. This process was directly observed [13] by a long-focus optical lens in experiments with vertical foam films suspended on a three-legs glass frame - in this configuration a single GPB is formed between the three films hanged on the frame legs [37]. Immediately after the withdrawal of the glass frame from the surfactant solution containing pre-emulsified antifoam, one observes numerous oil drops trapped in the just formed, thick foam films [13]. However, these oil drops are expelled out of the film almost instantaneously, because the film thickness becomes smaller than the drop diameter due to the liquid drainage. Fraction of these oil drops is trapped in the narrowing GPB - a drop entry and subsequent film rupture is observed when the GPB cross-section becomes smaller than the drop diameter and the compressing pressure exceeds the entry barrier of the drops. Numerous oil drops are seen captured in the GPBs of real foams as well, see Figure 9F. The process of foam destruction in the presence of oil drops (slow antifoams) is described in more detail in Refs. [13-16].

It is worthwhile mentioning that the actual mechanism(s) of foam destruction after the oil drops enter the surface of the GPBs is still unclear. One interesting experimental fact is that very often the foam destruction occurs through sudden avalanches of multiple bubble bursts in the top layer of the foam, separated by still periods. To explain this observation, a "compression-bursting" mechanism was suggested in Ref. [13], which implies that the entry of strongly compressed (deformed) droplets in the GPBs creates a mechanical shock (due to the release of surface energy in the moment of drop entry), which is able to destroy the neighboring foam films. The mechanical energy, released upon the foam films rupture, creates a propagating mechanical stress that might break the thinnest (less stable) foam films in the upper layer of the foam column.

5. Relation between the final foam height, entry barrier and drop size for slow antifoams. The experiments performed in Ref. [14] showed that the foam evolution in the presence of oil drops consists of several stages (see Figure 9E). In all cases, the foam destruction by slow antifoams was incomplete (in the time-scale of interest, ca. 2 hours) and a residual, very stable foam of certain height was observed. This final foam height, H_F, depended on both the system composition and oil drop size [13, 14]. The following consideration explains the magnitude of H_F by analyzing the relations between: (1) the drop entry barrier and the compressing capillary pressure, imposed by the shrinking walls of the GPBs; (2) the drop size and the cross-section of the GPBs.

The capillary pressure, which compresses the oil drops in the GPBs, gradually increases with the drainage of liquid from the foam. The condition for a hydrostatic equilibrium in the foam column requires the appearance of a vertical gradient of the capillary pressure, which opposes the gravity [2, 38]. At equilibrium, the capillary pressure at the top of the foam column should be approximately equal to the hydrostatic pressure [13, 38]

$$P_{CF}(H) \approx \Delta\rho g H \,, \tag{6}$$

where $\Delta\rho$ is the mass density difference of the aqueous and gaseous phases, g is the acceleration of gravity, and H is the height of the foam column, see Figure 9A. The capillary pressure determines the radius of curvature, R_P, of the GPB wall (Figure 9D)

$$R_P \approx \frac{\sigma_{AW}}{P_{CF}} \approx \frac{\sigma_{AW}}{\Delta\rho g H} \tag{7}$$

and hence, determines also the cross-section of the GPB. The radius of a sphere, inscribed in a GPB (i.e. touching its walls of radius R_P; Figure 9D), can be found from geometrical considerations [13, 16]

$$R_D^{MIN} = \left(\frac{2\sqrt{3}}{3} - 1\right) R_P \approx 0.15 \frac{\sigma_{AW}}{\Delta\rho g} \frac{1}{H} \tag{8}$$

The notation R_D^{MIN} is used in eq 8, because this presents, in fact, the minimal radius of a drop that can be compressed by the walls of the GPBs in a foam column of height H.

It is seen from eqs 6 and 8 that the compressing capillary pressure P_{CF} is higher and R_D^{MIN} is smaller, for taller foam columns. If the drops trapped in the GPBs have entry barrier $P_C^{CR} < P_{CF}(H)$ and radius $R_D > R_D^{MIN}$, then the foam destruction will begin after certain period of liquid drainage, because the asymmetric oil-water-air films will be unable to resist the compressing pressure imposed by the shrinking walls (Figure 9C). The foam destruction will continue until $P_{CF}(H)$ becomes approximately equal to P_C^{CR} (i.e., the asymmetric films become stable) or, alternatively, until the cross-section of the GPBs becomes larger than the drop radius, $R_D^{MIN} \geq R_D$ (i.e., when the oil drops are not compressed anymore by the GPB walls). Therefore, the final height of the foam column, H_F, reached as a result of the foam destruction by the oil drops (Figure 9E), must be close to the larger of the two estimates

$$H_F = \max\{H_{FP}, H_{FR}\} \tag{9}$$

$$H_{FP} = \frac{P_C^{CR}}{\Delta\rho g} \tag{10a}$$

$$H_{FR} = 0.15 \frac{\sigma_{AW}}{\Delta\rho g} \frac{1}{R_D} \tag{10b}$$

One can conclude from this analysis that if $H_{FP} > H_{FR}$, the final foam height, H_F, is determined mainly by the entry barrier - the oil drops are still compressed, but the asymmetric films are stable. On the contrary, if $H_{FP} < H_{FR}$, the final foam height is determined by the drop size, while the entry barrier is of secondary importance.

It is worthwhile noting several complications, that might be important in some systems. First, the entry barrier might strongly depend on the drop size in some cases (see Figure 11 and section III.B.1 below), so that the above two conditions are not entirely independent - P_C^{CR} should be regarded as a function of R_D. Second, due to the fact that most of the antifoam emulsions are rather polydisperse, one must be careful what average drop size is used in the above estimates. Also, a coalescence between the trapped oil drops may occur inside the GPBs, which would lead to an increase of the drop size and possibly, to reduction of the entry barrier and foam stability.

To check whether the above estimates, eqs 9 and 10, describe the real foams, we performed a series of parallel experiments with various surfactant-antifoam couples for determination of the entry barrier, P_C^{CR}, by FTT and of the final foam height, H_F, by the Ross-

Miles test. The results are summarized in Figure 10, where H_F is shown as a function of P_C^{CR} (see the figure caption for the specific systems). The results show that the theoretical linear relationship between P_C^{CR} and H_F, eq 10a, holds very well for $P_C^{CR} \geq 400$ Pa (see the dashed line in Figure 10). The further decrease of the entry barrier almost does not affect H_F which remains around 3-4 cm for $P_C^{CR} < 400$ (see the shaded area in Figure 10). As explained above, the reason for this result is that the GPBs in short foam columns are too wide to compress the emulsified oil drops. Indeed, one can estimate from eq 8 that $R_D^{MIN} \approx 13$ μm for $H_F = 3.5$ cm ($\sigma_{AW} \approx 30$ mN/m). The size-distribution of the drops was determined for one of the studied systems - SDP3S and silicone oil. The main fraction of drops fell in the size-range between 2 and 20 μm in radius, though single larger drops were also observed. The *number* averaged, arithmetic mean drop radius was around 5 μm, whereas the geometric mean radius was around 4 μm (the standard deviation, calculated for a log-normal size-distribution of the drops, was $\sigma_g \approx 2$). These results indicate that R_D in eq. 10b should represent the typical radius of the larger drops (which are most active as antifoam entities) in the size distribution curves. The calculations, showed that one could use the *volume* averaged, geometric mean drop size (which was $R_D \approx 16$ μm in these experiment) as a reasonable estimate of R_D in eq. 10b.

Equations 9 and 10 predict that one can use the entry barrier and/or the drop size, to control the final height of the foam. Indeed, FTT measurements showed that the addition of different amphiphiles (foam boosters, such as dodecanol, betaines, and others) to the main surfactant (e.g., SDS or SDP3S) leads to a significant increase of the entry barrier, at a fixed total surfactant concentration [13, 14]. The observed increase of the entry barriers was in a very good agreement with the enhanced foam stability found with the same systems in the foam tests. On the other side, the foam stability was found to increase noticeably with the reduction of the oil drop size, at fixed composition of the surfactant solution, just as predicted by the above consideration - cf. Figures 4 and 5 in Ref. [13].

B. Effect of Different Factors on the Drop Entry Barrier.

The above results clearly demonstrate the importance of the entry barrier for the activity of the oil-based antifoams. That is why, we made systematic experiments to clarify how the entry barrier depends on various factors.

1. Effect of the drop size. The FTT experiments with many different systems showed that, in general, P_C^{CR} monotonously decreases with the drop size. In many cases this trend is very weak (e.g., the results shown in Figure 3) and can be neglected for the size-range of typical antifoams (R_D between 1 and 10 μm), whereas in some systems the size effect is very pronounced. Interestingly, we found that the dependence of P_C^{CR} on the drop size is sensitive to the surfactant concentration. As an example, the dependence of P_C^{CR} on the equatorial drop radius, R_E, is shown on Figure 11 for silicone oil (viscosity 5 mPa.s) at three different concentrations of SDP3S. The radius of the studied drops varies between 1 and 8 μm. To compare quantitatively the effect of the drop size for the different concentrations, we define the ratio $p = P_C^{CR}(2\ \mu m) / P_C^{CR}(6\ \mu m)$, which shows how steep is the decrease of the entry barrier with the drop size. At the lowest concentration (5×10^{-4} M, which is around the CMC of this surfactant) the ratio $p \approx 1.1$; For the intermediate concentration (0.02 M), this ratio is slightly larger, $p \approx 1.3$; For a concentration which is far above the CMC (0.1 M) a significant increase of p is observed, $p \approx 2.9$, i.e. the entry barrier decreases about 3 times in the studied size-range. As discussed by the end of the previous section, this dependence can be used to control the foam stability by varying the size of the oil drops introduced into the foaming solution. Why is the

ratio p larger for more concentrated surfactant solutions is still an open question. The explanation might be in the different types of surface forces (electrostatic and van der Waals at low concentrations; oscillatory structural forces at high concentrations) which stabilize the asymmetric films in the different concentration ranges.

2. Effect of the surfactant concentration. A series of experiments is performed with SDDBS solutions of different concentrations to measure the entry barrier for hexadecane drops. The surfactant concentration, C_S, is varied between 0.16 and 12.8 mM, while the salt concentration is fixed at 12 mM NaCl. The CMC of SDDBS at this ionic strength is about 0.5 mM. The working solutions are poured in the experimental cell by using the two-tips procedure (TTP) described in section II.B.3c, to avoid the presence of a spread oil on the solution surface. The entry barriers, measured with oil drops of radius $R_E \approx 3 \pm 0.25$ μm, are plotted in Figure 12, as a function of the surfactant concentration. At least 3 independent experimental runs are carried out at a given concentration, with 2-3 entry events observed in each run. The reproducibility of the measured value of P_C^{CR} is very good, typically ± 5 %.

The results shown in Figure 12 indicate a complex dependence of P_C^{CR} on the surfactant concentration: At concentrations below 0.16 mM, the entry barrier is too low to be measured by the used experimental procedure. In this case the drops entered the solution surface without being necessary to compress them by the water-air interface. At the lowest concentration, where FTT measurements were possible, C_S = 0.16 mM, P_C^{CR} = 10 Pa is obtained. The entry barrier rapidly increases in the concentration range between 0.16 and 0.5 mM, up to ≈ 40 Pa. At higher concentrations, between 0.5 and 9 mM, the barrier exhibits a slow but steady increase from ca. 40 to 150 Pa with the surfactant concentration. A much steeper increase of P_C^{CR} is observed at concentrations above 9 mM and the barrier is above 400 Pa at C_S = 12.8 mM.

The observed sharp increase of P_C^{CR} at C_S > 9 mM is probably related to the stabilizing effect of the surfactant micelles trapped in the asymmetric oil-water-air film [3, 10]. One can estimate that the effective volume fraction of the SDDBS micelles, Φ, including the contribution of the counter-ion atmosphere, is about 6 % at the kink point of 9 mM [17]. From the micellar concentration one can estimate the height of the last maximum (corresponding to one layer of micelles trapped in the film) in the oscillatory component of the disjoining pressure, created by the micelles, by using the formulae derived in Ref. [36]. The estimate shows that this maximum is about 73 Pa, which is not far away from the measured values of $P_C^{CR} \approx 160$ Pa at this concentration (note that the electrostatic and van der Waals forces also contribute to the height of this maximum in the film). Therefore, a detectable contribution of micelles in the stability of the films might be expected in this concentration range and above it. More detailed discussion of these results is presented in Ref. [17].

3. Effect of the chemical structure of oil. All experiments described in sections III.B.3 and III.B.4 are carried out with solutions containing 2.6 mM SDDBS and 12 mM NaCl. The drop entry barriers for a series of n-alkanes (octane, decane, dodecane, hexadecane), dodecanol and silicone oil are measured. Drops of diameter between 2 μm and 12 μm are studied and no significant dependence of P_C^{CR} on the drop size is observed. The mean values of the drop entry barrier, P_C^{CR}, measured for the different oils, are summarized in Table 2. The values given in parentheses correspond to experiments performed in the absence of a spread oil layer over the solution surface, while the other values are measured with a pre-spread, molecularly thin oil layer on the solution surface. The results demonstrate that the entry barrier for n-alkanes increases with their molecular mass: for octane $P_C^{CR} = 30 \pm 2$ Pa, for decane 35 ± 5 Pa (> 70 Pa with solution surface free of spread oil), for dodecane 48 ± 5 Pa (96 ± 5 Pa), and for hexadecane it is 400 ± 10 Pa (80 ± 5 Pa). Such a significant increase of the entry barrier with the alkane

chain-length is certainly important for the antifoam action of the alkanes, and systematic foam tests are planned to understand better the relation between the entry barrier and the foam stability for these systems. The significant effect of the spread oil on the entry barrier, found with most of the alkanes, will be discussed in the next section.

The experiments with drops of n-dodecanol and silicone oil revealed very high entry barriers, above 1500 Pa. Not surprisingly, the foam tests showed that emulsified drops of both these oils are inefficient foam breakers, although the *E*, *S*, and *B* coefficients are strongly positive for the silicone oil [16]. More detailed discussion of these results, along with some possible explanations for the different entry barriers of the studied oils are presented in Ref. [17].

4. Effect of the pre-spread oil layers. The experiments with dodecane and decane demonstrated a significantly lower drop entry barrier in the presence of a pre-spread layer of the same oil on the solution surface. On the contrary, the spreading of hexadecane (which makes a mixed adsorption layer with the SDDBS molecules) leads to about fivefold increase of the entry barrier, as compared to that in the absence of spread oil (see Table 2). It is rather possible that the high entry barrier observed with dodecanol is also related to the formation of a dense mixed adsorption layer on the solution surface [16, 17]. Therefore, the presence of a spread oil layer is a significant factor for the magnitude of the entry barriers. Let us note that this effect has an important implication for the antifoaming action of these oils. For example, one could not explain the poor antifoam activity of hexadecane in SDDBS solutions, without taking into account the increase of the entry barrier due to the oil spreading. However, as discussed in Refs. [4, 5, 13, 16, 17, 39], different factors are often more important and no straightforward correlation between the spreading behavior of the oil and its antifoam activity is observed.

5. Discussion of the Critical Disjoining Pressure for Drop Entry. The results presented in Figures 3 and 11 show that the critical *capillary* pressure, P_C^{CR}, is usually a weak function of the size of the asymmetrical oil-water-air film. Additional analysis is needed, however, to understand how the critical *disjoining* pressure, Π_{AS}^{CR}, depends on the film size. In this section we investigate this dependence and discuss it from the viewpoint of the mechanism of rupture of the thin asymmetric films.

a. Disjoining pressure for spherical films. The disjoining pressure, Π_{AS}, accounts for the interactions between the two film surfaces (van der Waals, elctrostatic, steric, etc.) and is conventionally defined as the surface force per unit area [40-42]. Positive disjoining pressure corresponds to repulsive surface forces (i.e. to film stabilization) and vice versa. In the case of planar films, the condition for mechanical equilibrium requires that the capillary sucking pressure must be exactly counterbalanced by the disjoining pressure. However, the thin films in our experiments are curved and the condition for mechanical equilibrium is more complex, because it should account for the capillary pressure jumps across the curved film surfaces. The relevant theoretical approach to this configuration was developed by Ivanov and Kralchevsky [25, 42, 43], who showed that the disjoining pressure is related to the capillary pressure across the water-air interface, $P_C = P_A - P_W$, by the expression

$$\Pi_{AS} = P_F - P_W = (P_F - P_A) + (P_A - P_W) = \frac{2\sigma_{AW}}{R_F} + P_C \qquad (11)$$

where P_F is the pressure in the asymmetric oil-water-air film and R_F is its radius of curvature (Figure 13A). The aqueous phase (from which the asymmetric film is formed) is chosen as a referent phase for the definition of the disjoining pressure as usual [42, 43].

For micrometer sized drops R_F is on the order of the drop size and $2\sigma_{AW}/R_F > 10^4$ Pa. In most of our systems $P_C \approx 10^2$ Pa and its contribution can be neglected in eq 11. Thus only the

radius of film curvature, R_F, would be sufficient to calculate Π_{AS}, because σ_{AW} is a known quantity. Note, however, that R_F depends on the drop deformation, which in turn is determined by the applied capillary pressure, P_C. For large drops or bubbles, one can measure directly the radius of film curvature, R_F, by using the microscopic method of differential interferometry [44]; however, this method cannot be used for micrometer sized drops. That is why, an indirect method was used in Ref. [17] to estimate the magnitude of Π_{AS} from the accessible experimental data, and to study how the critical disjoining pressure for drop entry, Π_{AS}^{CR} depends on the size of the asymmetric film. We refrain from describing here the exact numerical procedure, because this would require too much space. Briefly, it consists in restoring the shape of the trapped oil drop and of the contiguous water-air meniscus from the accessible experimental data - the capillary pressure P_C, the equatorial drop radius R_E and the interfacial tensions, σ_{AW} and σ_{OW}. From the restored drop shape one finds R_F^{CR} and Π_{AS}^{CR} in the moment of film rupture. For detailed explanation of the numerical procedure, the reader is referred to the original article [17].

b. Numerical results. The calculated dependence of Π_{AS}^{CR} on the inverse radius of the asymmetric film is shown in Figure 13B, for the system 3.2 mM SDDBS, 12 mM NaCl, and hexadecane drops (no spread layer of oil). Since the asymmetric film is curved, there are different possible definitions of its size. For this plot we have chosen the "effective" film radius to be equal to the radius of a planar film, that has the same area as the real asymmetric film

$$R_{EFF} = \sqrt{A_F / \pi} \tag{12}$$

where A_F is the actual area of the asymmetric film. As seen from Figure 13B, Π_{AS}^{CR} is a linear function of $1/R_{EFF}$. The calculations performed in Ref. [17] showed that for a given system, the drop entry occurs at approximately the same relative deformation of the drops (independently of the drop size).

The observed dependence Π_{AS}^{CR} on R_{EFF} is by no means a trivial fact. The isotherm $\Pi_{AS}(h)$ is not expected to depend on either the film size or the film curvature, because the film thickness h is much smaller than both R_{EFF} and R_F. Therefore, if the film rupture were accomplished by surmounting the maximum in the isotherm $\Pi_{AS}(h)$, then the rupture event for a given system would be expected to occur always at $\Pi_{AS}^{CR} = \Pi_{AS}^{MAX}$, independently of the drop size.

One possible explanation of the observed dependence might be that the film rupture in our systems occurs by passing below the barrier Π_{MAX} (Figure 13C). Indeed, Bergeron [45] showed with large planar foam films (studied by the porous plate method) that in some systems Π^{CR} corresponded to an actual maximum of the calculated DLVO-curve $\Pi(h)$, while in other systems Π^{CR} was well below the maximum of the calculated $\Pi(h)$ curves (for a possible explanation see Ref. [45]). Such a possibility is offered by different theoretical models of film rupture, in which the formation of unstable spots in large liquid films by various mechanisms is considered [40, 45-47]. However, all these models are developed for large planar films and cannot be directly applied to our system without a careful analysis of the role of film curvature in the film rupture process. A further experimental and theoretical work is under way to reveal the actual mechanism of film rupture, to develop an adequate model of this process, and to explain the observed dependence $\Pi_{AS}^{CR}(R_{EFF})$.

IV. Conclusions.

A systematic experimental study is performed to clarify further the role of the entry barrier in the foam destruction by oil-based antifoams. The critical capillary pressure, P_C^{CR}, which leads to rupture of the asymmetric oil-water-air film (formed between a pre-emulsified oil drop and the solution surface) and to subsequent drop entry, is measured by the Film Trapping Technique (Figure 2) - for brevity, P_C^{CR} is denoted as "the entry barrier" throughout the paper. The obtained results and conclusions can be summarized in the following way:

1. The experiments reveal that P_C^{CR} determines the boundary between two different classes of antifoam (Figures 3 and 4):
   (a) Fast antifoams (defoaming time < 5 s, no residual foam), which have $P_C^{CR} < 20$ Pa and break the foam films (Figures 7 and 8).
   (b) Slow antifoams (defoaming time > 5 min, stable residual foam), which have $P_C^{CR} > 20$ Pa and destroy the foam only after being compressed inside the Gibbs-Plateau borders (Figures 6 and 9).
2. A relation between P_C^{CR}, the final height of the foam, H_F, and the radius of the antifoam drops, R_D, is found and explained theoretically for the slow antifoams (Figures 9 and 10).
3. The dependence of the entry barrier on the concentration of the anionic surfactant sodium dodecylbenzene sulfonate (SDDBS) is studied for hexadecane oil drops. A steep increase of the barrier is observed at concentration above 9 mM (effective volume fraction of the micelles ≈ 6 %), which implies that the oscillatory structure forces, created by the micelles, play a significant role above this concentration (Figure 12).
4. The presence of a pre-spread oil layer on the surface of the surfactant solution is found to affect strongly the entry barrier for alkanes (Table 2). The barrier is reduced by the pre-spread layer for decane and dodecane, whereas the effect is the opposite for hexadecane (fivefold increase).
5. There is a big difference between the numerical values of the critical *capillary* pressure, P_C^{CR}, and the critical *disjoining* pressure, Π_{AS}^{CR}, for micrometer sized oil drops, like those in real antifoams. The analysis shows that P_C^{CR} is a more convenient quantity for description of the entry barriers, because its magnitude correlates with the final height of the foam, whereas the magnitude of Π_{AS}^{CR} does not.
6. The experiments show that P_C^{CR} usually depends slightly on the oil drop size and on the radius of the asymmetric film, while Π_{AS}^{CR} scales as (film radius)$^{-1}$ for all of the studied systems (Figure 13B). The strong dependence of Π_{AS}^{CR} on the film radius shows that the rupture of the asymmetric film does not occur simply by surmounting the barrier in the $\Pi_{AS}(h)$ curve. A possible explanation of this result is discussed (Figure 13C).

One can conclude that the FTT has provided a valuable and non-trivial information about the role of entry barrier for the antifoam activity of oils and oil-based compounds.

References

1. PR Garrett ed. *Defoaming: Theory and Industrial Applications*. Surfactant Science Series. Marcel Dekker: New York, 1993, Vol. 45.
2. D Exerowa, PM Kruglyakov. In: *Foams and Foam Films*. Elsevier: Amsterdam, 1998, Chapter 9.
3. DT Wasan, SP Christiano, In: KS Birdi, ed. *Handbook of Surface and Colloid Chemistry*. CRC Press: Boca Raton FL, 1997, Chapter 6.
4. PR Garrett, In: PR Garrett, ed. *Defoaming: Theory and Industrial Applications*. Surfactant Science Series. Marcel Dekker: New York, 1993, Vol. 45, Chapter 1.
5. PR Garrett, J Davis, HM Rendall. *Colloids Surfaces A: Physicochem. Eng. Aspects* 85:159-197, 1994.
6. V Bergeron, P Cooper, C Fischer, J Giermanska-Kahn, D Langevin, A Pouchelon. *Colloids Surfaces A: Physicochem. Eng. Aspects* 122:103-120, 1997.
7. K Koczo, JK Koczone, DT Wasan. *J. Colloid Interface Sci*. 166:225-238, 1994.
8. R Aveyard, JH Clint. *J. Chem. Soc. Faraday Trans*. 91:2681-2697, 1995; R Aveyard, BP Binks, PDI Fletcher, TG Peck, PR Garrett. *J. Chem. Soc. Faraday Trans*. 89:4313-4321, 1993.
9. V Bergeron, ME Fagan, CJ Radke. *Langmuir* 9:1704-1713, 1993.
10. L Lobo, DT Wasan. *Langmuir* 9:1668-1677, 1993.
11. ND Denkov, P Cooper, J-Y Martin. *Langmuir* 15:8514-8529, 1999.
12. ND Denkov. *Langmuir* 15:8530-8542, 1999.
13. E Basheva, D Ganchev, ND Denkov, K Kasuga, N Satoh, K Tsujii. *Langmuir* 16:1000-1013, 2000.
14. E Basheva, S Stoyanov, ND Denkov, K Kasuga, N Satoh, K Tsujii. *Langmuir* 2000, in press.
15. ND Denkov, K Marinova. *Proceedings of the 3rd EuroConference on Foams, Emulsions and Applications*; MIT: Bremen, 2000.
16. L Arnaudov, ND Denkov, I Surcheva, P Durbut, G Broze, A Mehreteab. *Langmuir* 2000, submitted for publication.
17. A Hadjiiski, S Tcholakova, ND Denkov, P Durbut, G Broze, A Mehreteab. *Langmuir* 2000, submitted for publication.
18. PM Kruglyakov, TA Koretskaya. *Kolloid. Zh.* 36:682-686, 1974; PM Kruglyakov. In: IB Ivanov, ed. *Thin Liquid Films: Fundamentals and Applications*. Surfactant Science Series. Marcel Dekker: New York, 1988, Vol. 29, Chapter 11.
19. RD Kulkarni, ED Goddard, B Kanner. *J. Colloid Interface Sci.* 59:468-476, 1977.
20. K Koczo, LA Lobo, DT Wasan. *J. Colloid Interface Sci.* 150:492-506, 1992.
21. KJ Mysels, MN Jones. *Disc. Faraday Soc*. 42:42-50, 1966.
22. A Hadjiiski, R Dimova, ND Denkov, IB Ivanov, R Borwankar. *Langmuir* 12:6665-6675, 1996.
23. SM Patrick, H An, MB Harris, IB Ivanov, NS Braunshtein, EF Leonard. *Annals Biomed. Engin.* 25:1072-1079, 1997.
24. IB Ivanov, A Hadjiiski, ND Denkov, TD Gurkov, PA Kralchevsky, S Koyasu. *Biophys. J.* 75:545-556, 1998.
25. A Hadjiiski, S Tcholakova, IB Ivanov, TD Gurkov, E Leonard. *Langmuir* 2000, submitted.
26. A Scheludko, D Exerova. *Kolloid Z.* 165:148-151, 1959.
27. A Scheludko. *Adv. Colloid Interface Sci.* 1:391-464, 1967.

28. AS Aronson. *Langmuir* 2:653-659, 1986.
29. A Dippenaar. *Int. J. Miner. Process.* 9:1-14, 1982.
30. P Garrett. *Langmuir* 11:3576-3584, 1995.
31. AD Nikolov, DT Wasan, PA Kralchevsky, IB Ivanov. In: N Ise, I Sogami, eds. *Ordering and Organization in Ionic Solutions*. World Scientific: London, 1988, pp 302-314.
32. AD Nikolov, DT Wasan, PA Kralchevsky, IB Ivanov. *J. Colloid Interface Sci.* 133:1-12, and 133:13-22, 1989.
33. DT Wasan, AD Nikolov, PA Kralchevsky, IB Ivanov. *Colloids Surfaces* 67:139-145, 1992.
34. V Bergeron, CJ Radke. *Langmuir* 8:3020-3026, 1992.
35. ML Pollard, CJ Radke. *J. Chem. Phys.* 101:6979-6991, 1994.
36. PA Kralchevsky, ND Denkov. *Chem. Phys. Lett.* 240:385-392, 1995.
37. K Koczo, G Racz. *Colloids Surfaces* 22:97-110, 1987.
38. G Narsimhan, E Ruckenstein. In: RK Prud'homme, SA Khan, eds. *Foams: Theory, Measurements, and Applications*. Surfactant Science Series. Marcel Dekker: New York, 1996, Vol. 57, Chapter 2.
39. K Marinova, ND Denkov. *Langmuir* 2000, submitted for publication.
40. BV Derjaguin. *Theory of Stability of Colloids and Thin Liquid Films*. Plenum, Consultants Bureau: New York, 1989, Chapter 12.
41. IB Ivanov, BV Toshev. *Colloid Polymer Sci.* 253:558-565 and 253:593-599, 1975.
42. IB Ivanov, PA Kralchevsky. In: IB Ivanov, ed. *Thin Liquid Films: Fundamentals and Applications*. Surfactant Science Series. Marcel Dekker: New York, 1988, Vol. 29, Chapter 2.
43. PA Kralchevsky. *Effect of Film Curvature on the Thermodynamic Properties of Thin Liquid Films*. Ph. D. Thesis: Sofia University, Sofia, Bulgaria, 1984 [In Bulgarian].
44. AD Nikolov, PA Kralchevsky, IB Ivanov. *J. Colloid Interface Sci*. 112:122-131, 1986.
45. V Bergeron. *Langmuir* 13:3474-3482, 1997.
46. D Kaschiev, D Exerowa. *J. Colloid Interface Sci.* 77:501-511, 1980.
47. PA Kralchevsky, AD Nikolov, DT Wasan, IB Ivanov. *Langmuir* 6:1180-1189, 1990.

Table 1. Composition of the studied surfactant solutions and critical micellization concentration (CMC) of the surfactants.

Surfactant	Surfactant concentration, mM	CMC, mM	Electrolyte concentration, mM
AOT	10	3	no
APG	0.45	0.15	10
Triton X-100	1	0.18	no
SDP3S	0.5; 20; 100	0.5	0.33; 13.2; 66
SDP3S/Betaine (80/20 molar ratio)	100	< 0.5	81
SDP3S/n-dodecanol (97/3 molar ratio)	100	< 0.5	no
SDDBS	0.16 - 12.8	0.5	12
SDS	20	8	no
SDS/n-dodecanol (97/3 molar ratio)	20	< 8	no

Table 2. Drop entry barrier, P_C^{CR}, measured with different oils in the presence or in the absence (data in parentheses) of spread oil on the surface of the aqueous solution, which contains 2.6 mM SDDBS and 12 mM NaCl.

Oil	$\boldsymbol{P_C^{CR}}$**, Pa**
n-octane	30 ± 2
n-decane	35 ± 5 (> 70)
n-dodecane	48 ± 5 (96 ± 5)
n-hexadecane	400 ± 10 (80 ± 5)
n-dodecanol	> 1 500
PDMS	> 3 000

Figure Captions

Figure 1. Formation of asymmetric oil-water-air films (shaded areas) in some of the possible mechanisms of foam destruction by oil drops or lenses: bridging-stretching (A-C-D) and (B-C-D) [11, 12]; bridging-dewetting (A-C-E) and (B-C-E) [2-6].

Figure 2. Scheme of the experimental setup and the basic principles of operation of the Film Trapping Technique, FTT [25]: (A) Vertical capillary, partially immersed in surfactant solution containing oil drops, is held close above the bottom of the experimental vessel. (B) The air pressure inside the capillary, P_A, is increased and the water-air meniscus in the capillary is pressed against the glass substrate. Some of the oil drops remain trapped in the wetting glass-water-air film and are compressed by the meniscus. At a given critical capillary pressure (see section II.B.3 for details) the asymmetric film formed between the oil drop and the solution surface ruptures and a drop entry event is observed by an optical microscope. (C) Another modification called "gentle FTT" is used for measuring entry barriers lower than 20 Pa - a flat meniscus is formed, which allows the trapping of drops at virtually zero capillary pressure.

Figure 3. Drop entry barrier versus drop radius measured by gentle FTT for solution of 10 mM AOT: pure silicone oil (empty circles), and silica-PDMS compound (filled triangles). The horizontal lines represent the respective average values.

Figure 4. Correlation between the entry barrier and the foam lifetime measured for different systems (see also Table 1): (1-6) 10 mM AOT and different silica-PDMS compounds; (7) 0.45 mM APG and silica-PDMS compound; (8-10) 1 mM Triton X-100 and different silica-PDMS compounds; (11-13) 0.1, 0.02, and 5×10^{-4} M SDP3S and silicone oil; (14) 0.1 M SDP3S/Betaine = 80/20 molar ratio and silicone oil; (15) 0.1 M SDP3S/n-dodecanol = 97/3 molar ratio and silicone oil; (16) 0.02 M SDS and silicone oil; (17) 0.02 M SDS/n-dodecanol = 97/3 molar ratio and silicone oil.

Figure 5. Stages of foam film thinning: (A)-(F) Schematic presentation; (B')-(F') photographs made in reflected light, which show the typical interference pattern for the corresponding stage, as observed in the capillary cell with 0.1 M SDP3S solution, containing 0.1 wt % silicone oil; bar 100 μm. (A) Two concave surfaces approach each other; (B) Formation of a film with a thicker central region called "dimple"; (C) An almost planar film crossed by several thicker regions (channels); (D) Film of average thickness around 120 nm; the channels almost disappear. All drops are expelled from the film; (E) A stepwise thinning of the film through formation and expansion of thinner (darker) spots - stratification. The arrows in (E') show the film areas containing different numbers of micelle layers, as indicated by the integers; (F) The film area is occupied by an equilibrium black film.

Figure 6. A photograph showing oil drops, which are expelled from the foam film into the surrounding Gibbs-Plateau border. The photograph is made in transmitted light to have a good contrast for the oil drops - under these conditions the boundary between the film and the Gibbs-Plateau border is not well seen (this boundary is indicated by a dashed arc). The solution is 0.1 M SDP3S and contains 0.1 wt % silicone oil; the bar is 20 μm.

Figure 7. Interference pattern ("fish-eye", pointed by the arrow), indicating the formation of an oil bridge in a foam film just before its rupture in the capillary cell. The film is made from 10

mM AOT solution containing 0.01 wt % silica-PDMS compound.

Figure 8. Formation and stretching of an oil bridge: (A-D) schematic presentation; (A'-D') photographs of the corresponding stages made with the Dippenaar cell.

Figure 9. Foam destruction by oil drops (slow antifoams) [13, 14]: (A, B) The oil drops are rapidly expelled from the foam films into the neighboring Gibbs-Plateau borders (GPBs) soon after the foam is formed; (C) The larger drops are strongly compressed in the narrowing GPBs and asymmetric oil-water-air films are formed; (D) Drops of radius smaller than R_D^{MIN} remain non-compressed and cannot induce foam rupture; (E) Schematic presentation of the main stages of foam evolution in the presence of oil drops - (I) drainage of liquid without bubble coalescence; (II) stable foam due to the insufficient compression of the oil drops; (III) foam destruction as a result of drop entry in the GPBs; (IV) long living residual foam with final height H_F; (F) Photograph of real foam cells with many oil drops trapped in the GPBs.

Figure 10. Final foam height, H_F, versus P_C^{CR} for different systems: (1-3) 5×10^{-4}, 0.02, and 0.1 M SDP3S; (4) 0.1 M SDP3S/Betaine = 80/20 molar ratio; (5) 0.1 M SDP3S/n-dodecanol = 97/3 molar ratio; (6) 0.02 M SDS; (7) 0.1 M SDS/n-dodecanol = 97/3 molar ratio.

Figure 11. Entry barrier, P_C^{CR}, for silicone oil as a function of the oil drop radius measured at three different concentrations of SDP3S.

Figure 12. Dependence of the entry barrier, P_C^{CR}, on the SDDBS concentration, C_S, for hexadecane drops. All solutions contain 12 mM NaCl. The entry barriers are measured with drops of radius $R_E = 2.3 \pm 0.3$ μm. The solution surface is free of oil.

Figure 13. Determination of the disjoining pressure Π_{AS} in the asymmetric oil-water-air film [17]. (A) Schematic presentation of an oil drop trapped in wetting film; $P_W + \Pi_{AS} = P_F$ is the pressure in the asymmetric film; (B) Calculated critical disjoining pressure Π_{AS}^{CR} as a function of the inverse effective film radius $1/R_{EFF}$, see Eq. (12); the circles show calculated values from experiments with different oil drops and the line represents the respective linear fit; the calculations are made for 1 mM SDDBS solution containing 12 mM NaCl and n-hexadecane drops; (C) Schematic presentation of the disjoining pressure isotherm $\Pi_{AS}(h)$. Two possible ways for overcoming the barrier and possible film rupture are indicated: (1) The film surfaces are compressed toward each other by a capillary pressure that drives the system to surmount the barrier Π_{MAX} - in this case, the critical disjoining pressure Π_{AS}^{CR} should be equal to Π_{MAX} independently of drop radius. (2) A local fluctuation in the film leads to the formation of unstable spot and local film rupture. In this case, the latter may occur at a critical disjoining pressure $\Pi_{AS}^{CR} < \Pi_{MAX}$ and hence, Π_{AS}^{CR} could depend on the film size.

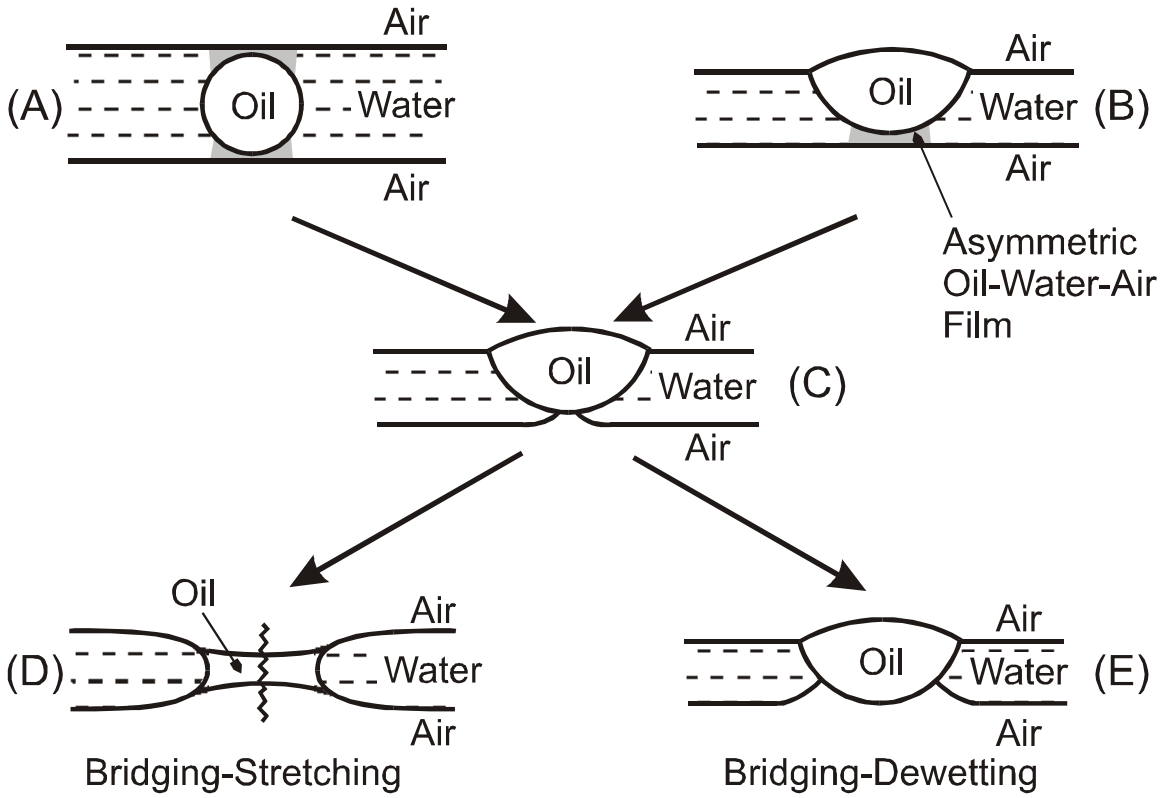

Figure 1. Formation of asymmetric oil-water-air films (shaded areas) in some of the possible mechanisms of foam destruction by oil drops or lenses: bridging-stretching (A-C-D) and (B-C-D) [11, 12]; bridging-dewetting (A-C-E) and (B-C-E) [2-6].

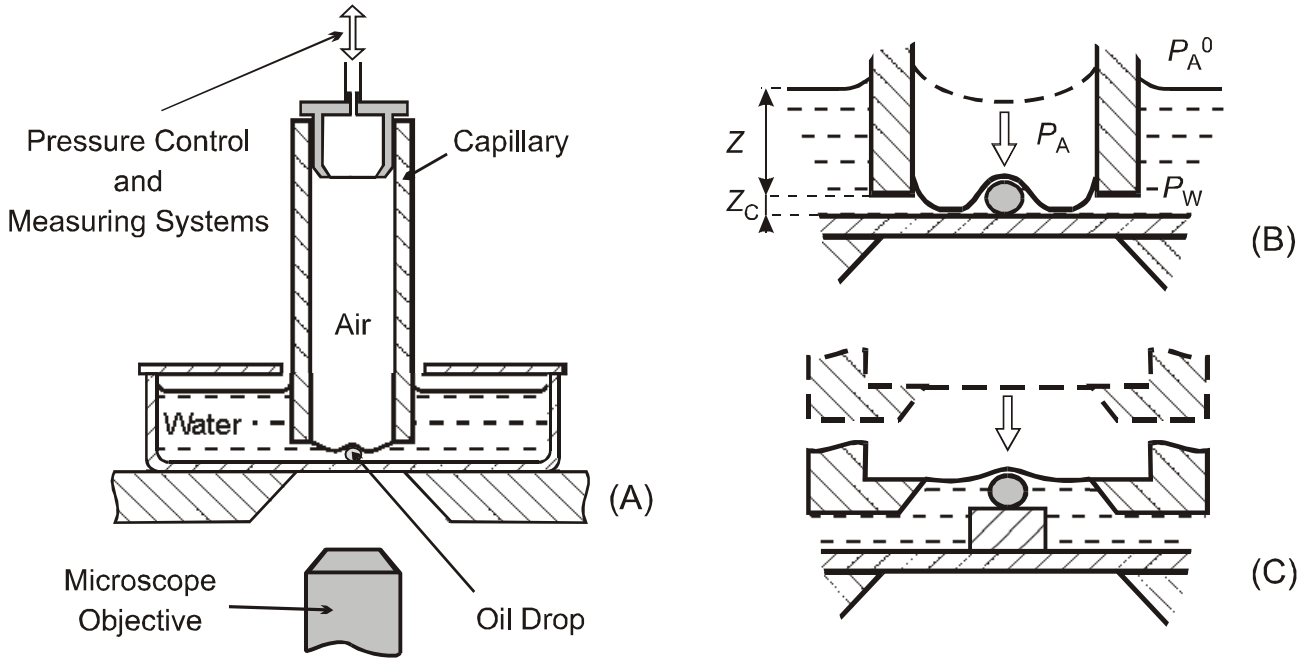

Figure 2. Scheme of the experimental setup and the basic principles of operation of the Film Trapping Technique, FTT [25]: (A) Vertical capillary, partially immersed in surfactant solution containing oil drops, is held close above the bottom of the experimental vessel. (B) The air pressure inside the capillary, P_A, is increased and the water-air meniscus in the capillary is pressed against the glass substrate. Some of the oil drops remain trapped in the wetting glass-water-air film and are compressed by the meniscus. At a given critical capillary pressure (see section II.B.3 for details) the asymmetric film formed between the oil drop and the solution surface ruptures and a drop entry event is observed by an optical microscope. (C) Another modification called "gentle FTT" is used for measuring entry barriers lower than 20 Pa - a flat meniscus is formed, which allows the trapping of drops at virtually zero capillary pressure.

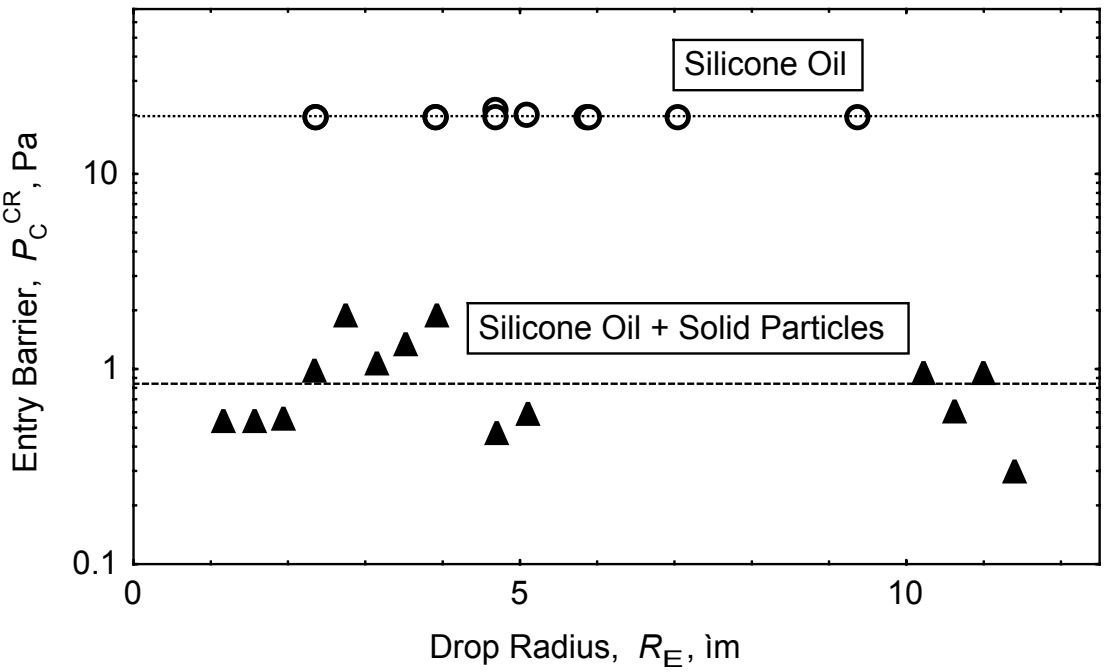

Figure 3. Drop entry barrier versus drop radius measured by gentle FTT for solution of 10 mM AOT: pure silicone oil (empty circles), and silica-PDMS compound (filled triangles). The horizontal lines represent the respective average values.

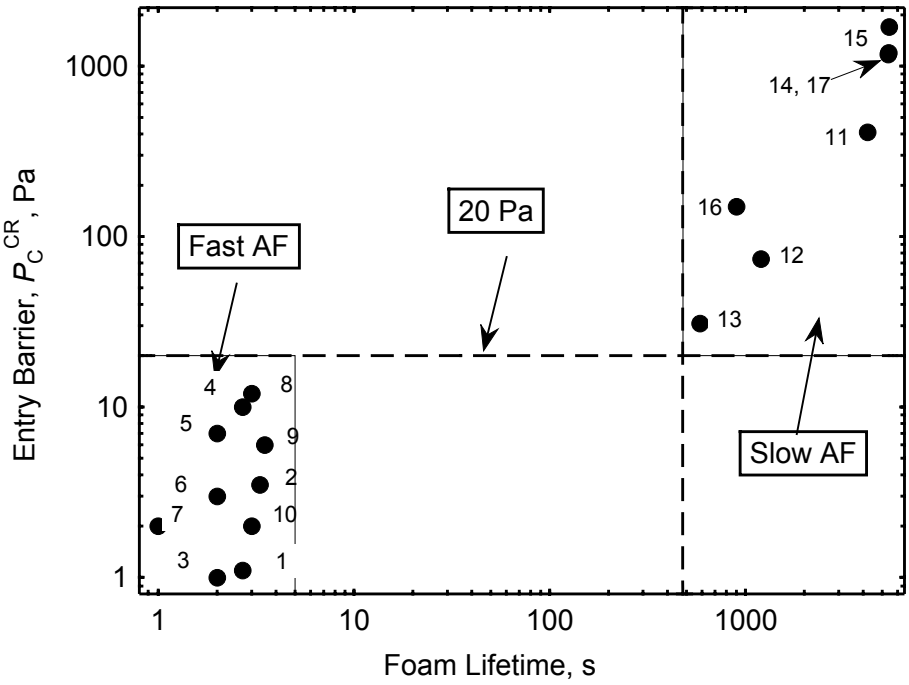

Figure 4. Correlation between the entry barrier and the foam lifetime measured for different systems (see also Table 1): (1-6) 10 mM AOT and different silica-PDMS compounds; (7) 0.45 mM APG and silica-PDMS compound; (8-10) 1 mM Triton X-100 and different silica-PDMS compounds; (11-13) 0.1, 0.02, and 5×10^{-4} M SDP3S and silicone oil; (14) 0.1 M SDP3S/Betaine = 80/20 molar ratio and silicone oil; (15) 0.1 M SDP3S/n-dodecanol = 97/3 molar ratio and silicone oil; (16) 0.02 M SDS and silicone oil; (17) 0.02 M SDS/n-dodecanol = 97/3 molar ratio and silicone oil.

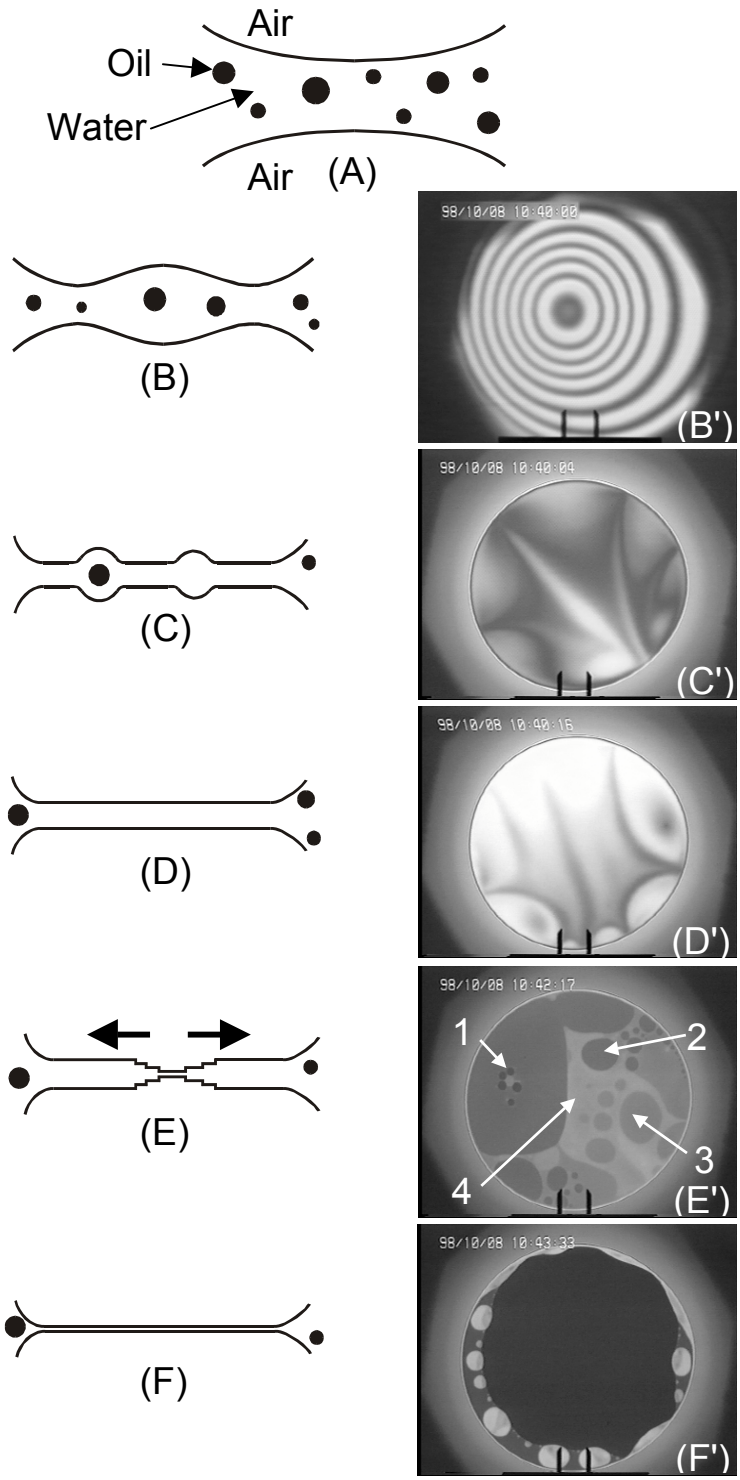

Figure 5. Stages of foam film thinning: (A)-(F) Schematic presentation; (B')-(F') photographs made in reflected light, which show the typical interference pattern for the corresponding stage, as observed in the capillary cell with 0.1 M SDP3S solution, containing 0.1 wt % silicone oil; bar 100 μm. (A) Two concave surfaces approach each other; (B) Formation of a film with a thicker central region called "dimple"; (C) An almost planar film crossed by several thicker regions (channels); (D) Film of average thickness around 120 nm; the channels almost disappear. All drops are expelled from the film; (E) A stepwise thinning of the film through formation and expansion of thinner (darker) spots - stratification. The arrows in (E') show the film areas containing different numbers of micelle layers, as indicated by the integers; (F) The film area is occupied by an equilibrium black film.

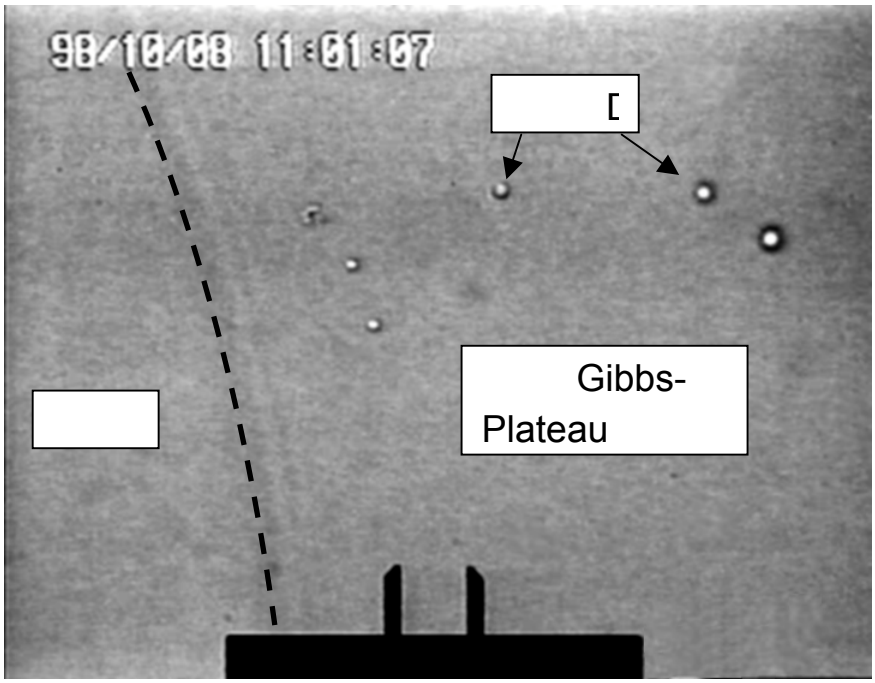

Figure 6. A photograph showing oil drops, which are expelled from the foam film into the surrounding Gibbs-Plateau border. The photograph is made in transmitted light to have a good contrast for the oil drops - under these conditions the boundary between the film and the Gibbs-Plateau border is not well seen (this boundary is indicated by a dashed arc). The solution is 0.1 M SDP3S and contains 0.1 wt % silicone oil; the bar is 20 μm.

Figure 7. Interference pattern ("fish-eye", pointed by the arrow), indicating the formation of an oil bridge in a foam film just before its rupture in the capillary cell. The film is made from 10 mM AOT solution containing 0.01 wt % silica-PDMS compound.

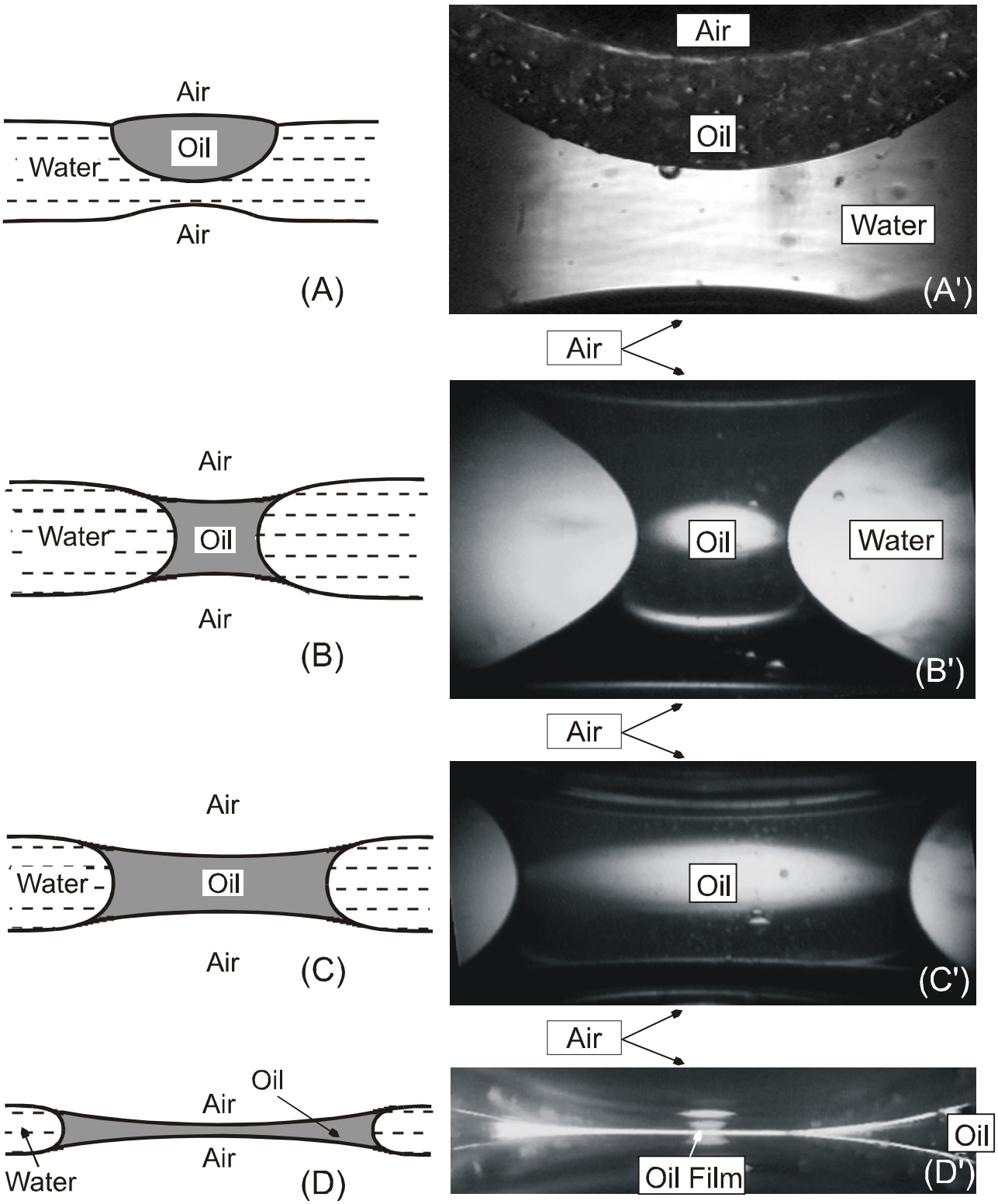

Figure 8. Formation and stretching of an oil bridge: (A-D) schematic presentation; (A'-D') photographs of the corresponding stages made with the Dippenaar cell.

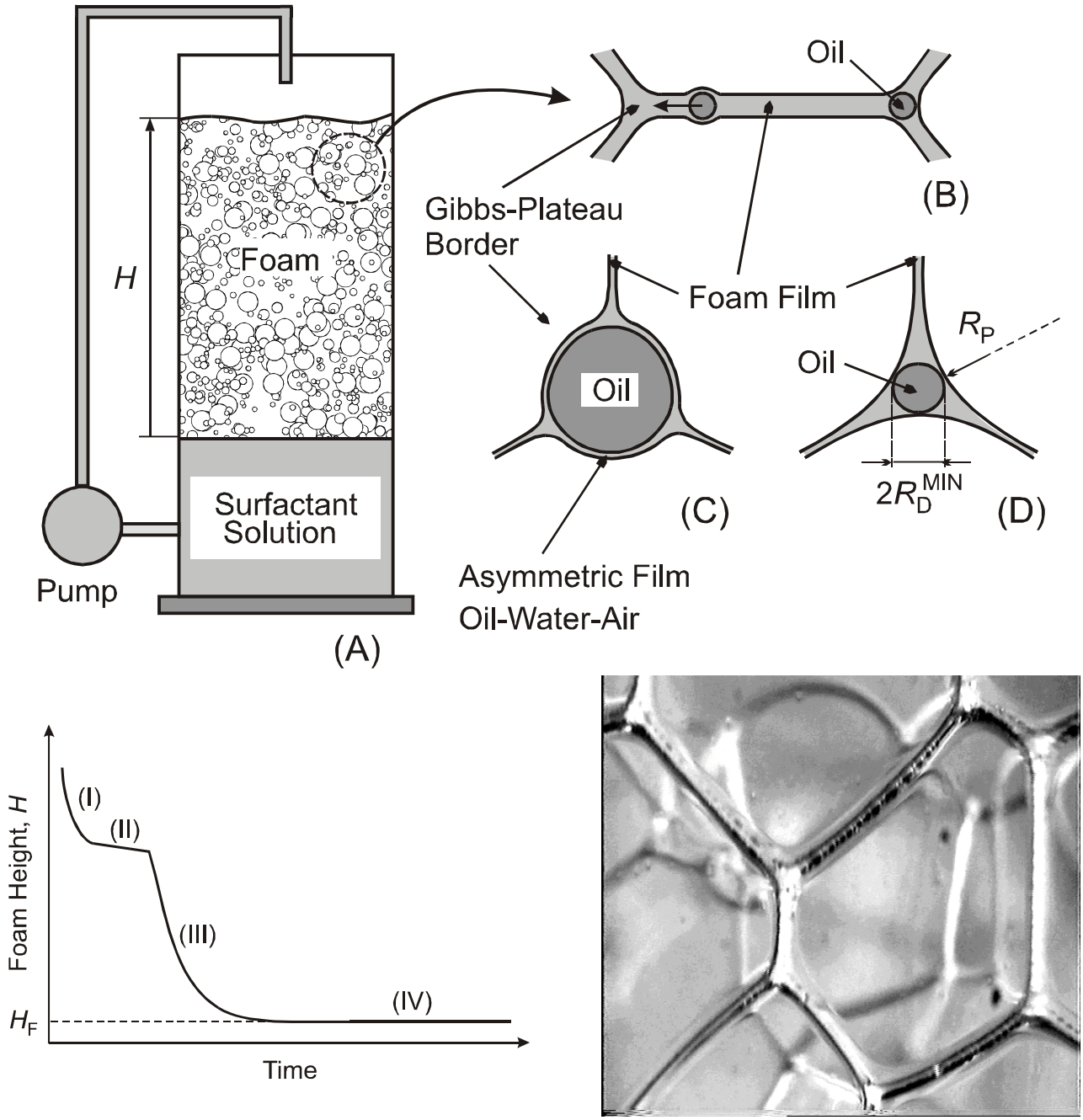

Figure 9. Foam destruction by oil drops (slow antifoams) [13, 14]: (A, B) The oil drops are rapidly expelled from the foam films into the neighboring Gibbs-Plateau borders (GPBs) soon after the foam is formed; (C) The larger drops are strongly compressed in the narrowing GPBs and asymmetric oil-water-air films are formed; (D) Drops of radius smaller than R_D^{MIN} remain non-compressed and cannot induce foam rupture; (E) Schematic presentation of the main stages of foam evolution in the presence of oil drops - (I) drainage of liquid without bubble coalescence; (II) stable foam due to the insufficient compression of the oil drops; (III) foam destruction as a result of drop entry in the GPBs; (IV) long living residual foam with final height H_F; (F) Photograph of real foam cells with many oil drops trapped in the GPBs.

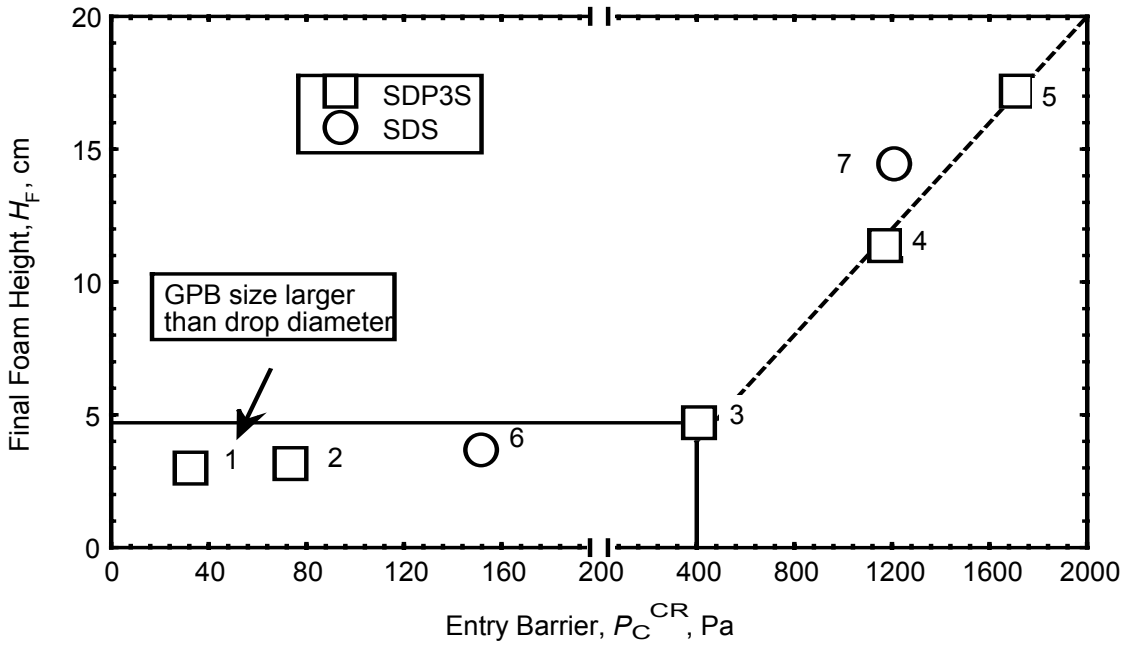

Figure 10. Final foam height, H_F, versus P_C^{CR} for different systems: (1-3) 5×10^{-4}, 0.02, and 0.1 M SDP3S; (4) 0.1 M SDP3S/Betaine = 80/20 molar ratio; (5) 0.1 M SDP3S/n-dodecanol = 97/3 molar ratio; (6) 0.02 M SDS; (7) 0.1 M SDS/n-dodecanol = 97/3 molar ratio.

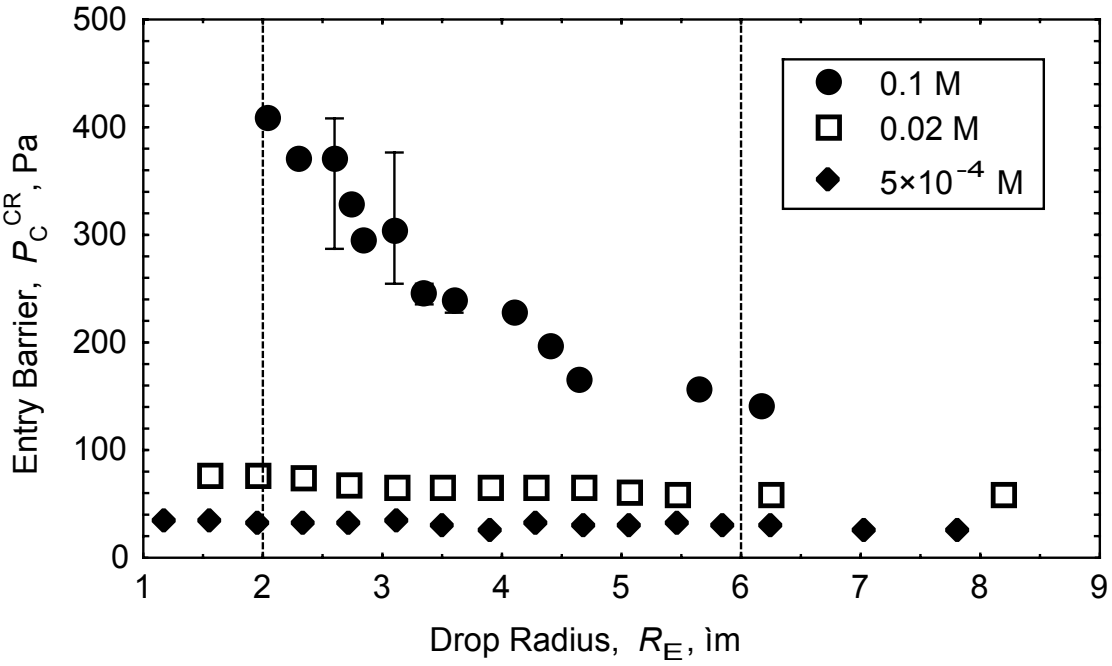

Figure 11. Entry barrier, P_C^{CR}, for silicone oil as a function of the oil drop radius measured at three different concentrations of SDP3S.

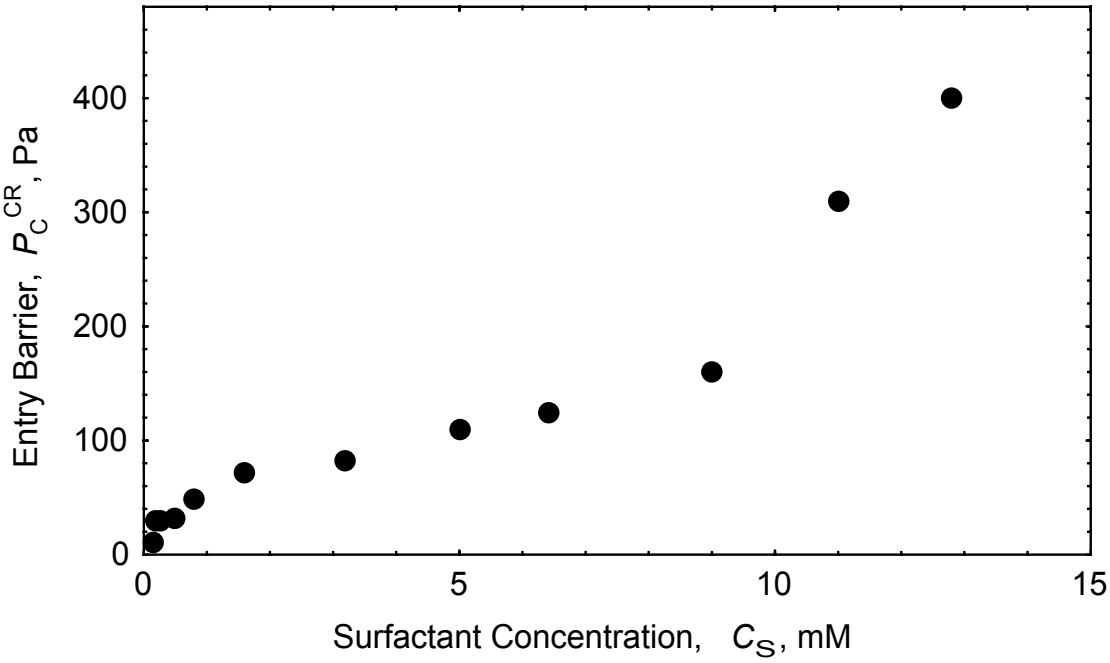

Figure 12. Dependence of the entry barrier, P_C^{CR}, on the SDDBS concentration, C_S, for hexadecane drops. All solutions contain 12 mM NaCl. The entry barriers are measured with drops of radius $R_E = 2.3 \pm 0.3$ μm. The solution surface is free of oil.

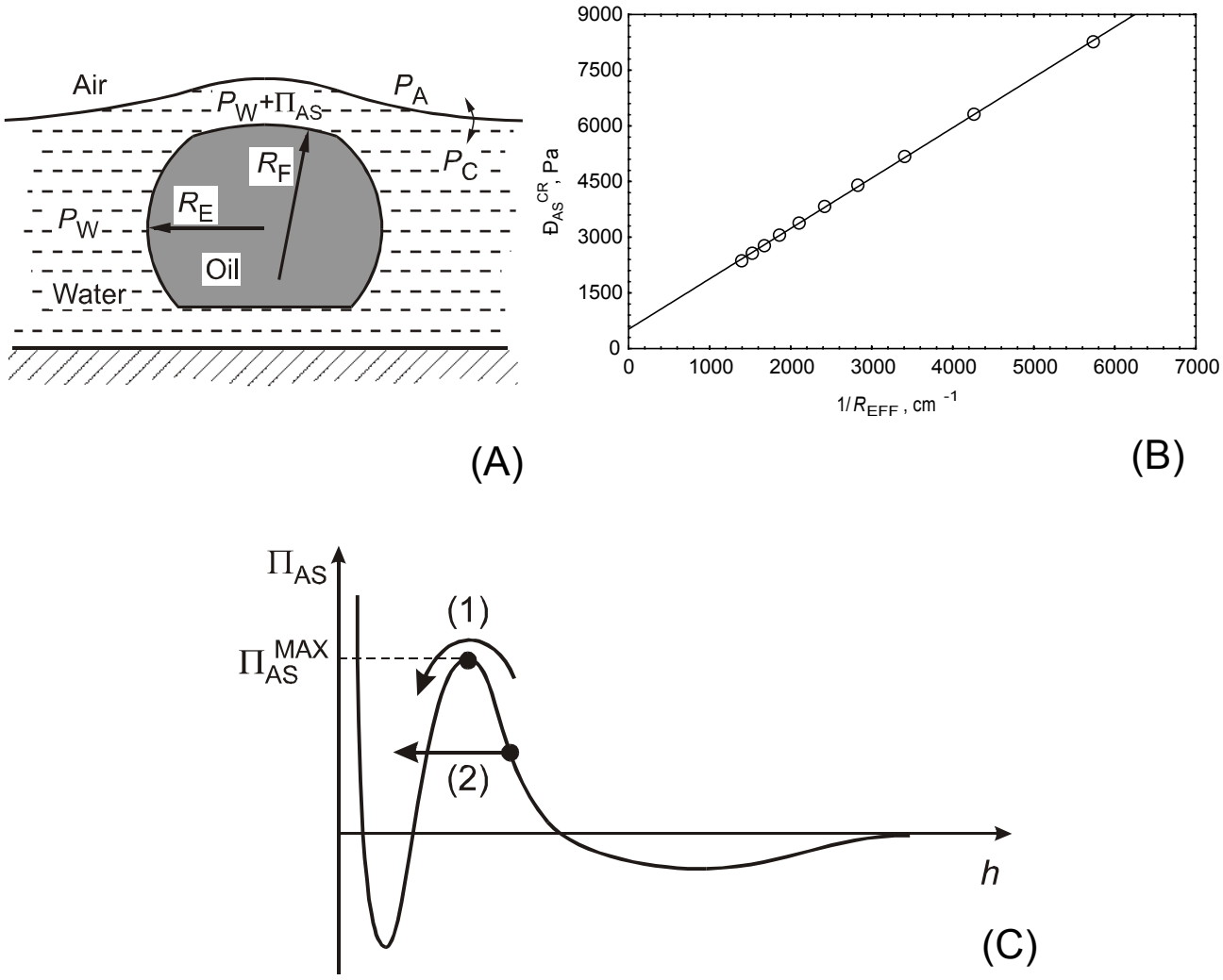

Figure 13. Determination of the disjoining pressure Π_{AS} in the asymmetric oil-water-air film [17]. (A) Schematic presentation of an oil drop trapped in wetting film; $P_W + \Pi_{AS} = P_F$ is the pressure in the asymmetric film; (B) Calculated critical disjoining pressure Π_{AS}^{CR} as a function of the inverse effective film radius $1/R_{EFF}$, see Eq. (12); the circles show calculated values from experiments with different oil drops and the line represents the respective linear fit; the calculations are made for 1 mM SDDBS solution containing 12 mM NaCl and n-hexadecane drops; (C) Schematic presentation of the disjoining pressure isotherm $\Pi_{AS}(h)$. Two possible ways for overcoming the barrier and possible film rupture are indicated: (1) The film surfaces are compressed toward each other by a capillary pressure that drives the system to surmount the barrier Π_{MAX} - in this case, the critical disjoining pressure Π_{AS}^{CR} should be equal to Π_{MAX} independently of drop radius. (2) A local fluctuation in the film leads to the formation of unstable spot and local film rupture. In this case, the latter may occur at a critical disjoining pressure $\Pi_{AS}^{CR} < \Pi_{MAX}$ and hence, Π_{AS}^{CR} could depend on the film size.